Published in final edited form as:

Neuron. 2020 October 28; 108(2): 302–321. doi:10.1016/j.neuron.2020.10.011.

Recent advances in electrical neural interface engineering: minimal invasiveness, longevity and scalability

Lan Luan[1,2,3], **Jacob T. Robinson**[1,2,3], **Behnaam Aazhang**[1,3], **Taiyun Chi**[1], **Kaiyuan Yang**[1], **Xue Li**[1,3], **Haad Rathore**[3,4], **Amanda Singer**[3,4], **Sudha Yellapantula**[1,3], **Yingying Fan**[1], **Zhanghao Yu**[1], **Chong Xie**[1,2,3]

[1] -Department of Electrical and Computer Engineering, Rice University, Houston, TX

[2] -Department of Bioengineering, Rice University, Houston, TX

[3] -NeuroEngineering Initiative, Rice University, Houston, TX

[4] -Applied Physics Graduate Program, Rice University, Houston, TX

Abstract

Electrical neural interfaces serve as direct communication pathways that connect the nervous system with the external world. Technological advances in this domain are providing increasingly more powerful tools to study, restore, and augment neural functions. Yet, the complexities of the nervous system give rise to substantial challenges in the design, fabrication and system-level integration of these functional devices. In this review, we present snapshots of the latest progresses in electrical neural interfaces, with an emphasis on advances that expand the spatiotemporal resolution and extent of mapping and manipulating brain circuits. We include discussions of large-scale, long-lasting neural recording, wireless, miniaturized implants, signal transmission, amplification and processing, as well as the integration of interfaces with optical modalities. We outline the background and rationale of these developments and share insights into the future directions and new opportunities they enable.

Graphical Abstract

Editorial correspondence: Chong Xie, Rice University, 6500 Main ST, 871, Houston, TX 77030, Phone: 713-348-8737, chongxie@rice.edu.

Author Contributions: C.X. led and organized the writing of this review, L.L., X.L. and C.X. wrote the section of *Intracortical electrode design*, J.T.R. and A.S. wrote the section of *Power, data, and communication*, T.C., K.Y., Y.F., and Z.Y. wrote the section of *Electronics for neural interfaces*, L.L. and H.R. wrote the section of *Bi-modal electrical-optical neural interfaces*, L.L., B. A., S.Y. and H.R. wrote the section of *From signals to key features: neural data processing*, all authors discussed and revised the manuscript.

Prepared as a review for Neuron after consultation with Dr. Rashmi Sarnaik.

Declaration of Interests: C.X. and L.L. are co-inventors on a patent filed by the University of Texas on a type of ultraflexible neural electrode technology discussed in the review. L.L. and C. X. hold equity ownership in Neuralthread Inc., an entity that is licensing this technology. A.S., K.Y. and J.R.R. are co-inventors on a pending patent filed by Rice University on magnetoelectric biodevices. All other authors declare no competing interests.

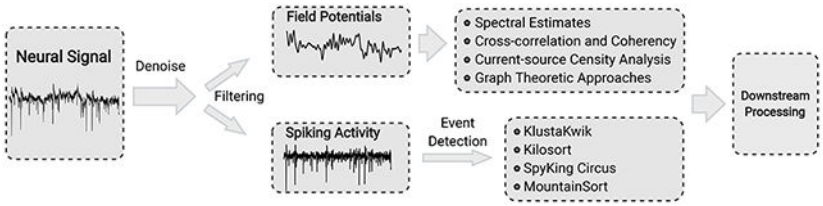

In Brief:

In this review, Luan, *et al*, discuss the latest advances in engineering electrical neural interfaces that expand the spatiotemporal resolution and extent of mapping and manipulating brain circuits, covering implanted devices, integrated circuits, signal transmission and processing.

Introduction

Perception, cognition and behavior are generated by complex, distributed neural circuits, the activity patterns of which change on the timescale of milliseconds. The dynamics of these activity patterns reflect complex interactions among many cell types, and they evolve with experience and change in disease. Three characteristics of these circuits make them particularly challenging to study: diversity of time scales, diversity of spatial scales, and heterogeneity. Devices that interface with the brain must therefore span these temporal and spatial scales in a scalable manner, while being able to address cell-type and regional diversity to account for species and individual variations (Box 1).

In the past few years, scientists and engineers have made cutting-edge technological advances to tackle these outstanding challenges. While these neurotechnological developments span a wide variety of research fields, such as microscopy, optical and genetic techniques, single-cell genomic profiling and connectomics, electrical interfaces are of paramount importance for both fundamental neuroscience and clinical applications. An electrical neural interface typically consists of an implanted device directly in touch with the brain, integrated circuits and mechanisms to transmit signals from and to the implant, and specialized algorithms to process these signals (Fig. 1). In this review, we discuss challenges and advances in designing the various components of an electrical neural interface that improve the capacity and efficacy with which we can monitor and manipulate neural activity. First, we discuss electrode design and strategies for long-term and large-scale recordings. Next, we address the need for electronics to be custom-designed for wireless, bi-directional transfer of data and power to the device. Then we outline how combination of electrical and optical methods widens possibilities to address the demands of spatio-temporal scale. Finally, we elaborate on the analytical methods to extract features from large-scale electrical recordings. Taken together, this review presents snapshots of the latest advances on electrical neural interface from a system-engineering perspective.

Intracortical electrode design

Implanted intracortical electrodes enable the detection of individual neurons at high temporal resolution in living brains (Alivisatos et al., 2012; Birmingham et al., 2014; Collinger et al., 2013; Nicolelis, 2001; Perlmutter and Mink, 2006; Shen, 2013; Spira and

Hai, 2013), and provide one of the most important neural techniques in the field (Lemon, 1984). Typically, individually addressed microscale electrodes are implanted into a designated brain region and connected to data acquisition systems. The recording sites transduce signals that arise from the current flow through the extracellular space during the propagation of action potentials, providing sufficiently high temporal resolution to resolve the activity of individual neurons residing in the immediate vicinity of the contacts.

Long-lasting functionality

Classic intracortical electrodes, are often impeded by the inability to consistently record high quality neural signals over both short and long time scales (Fraser and Schwartz, 2012; Perge et al., 2013). In time scales as short as minutes (Gilletti and Muthuswamy, 2006) and hours (Fraser and Schwartz, 2012; Perge et al., 2013), substantial changes in recording condition can often occur due to the micro-movements of the implanted electrodes relative to the brain tissue (Gilletti and Muthuswamy, 2006). Over longer periods, deteriorations in recording efficacy and fidelity typically appear a few weeks after implantation, which are caused by biotic and abiotic failures, including material and structural degradation of the electrodes (Gilgunn et al., 2013; Kozai et al., 2015a; Prasad et al., 2014; Prasad et al., 2012), and sustained foreign body reactions at the tissue-probe interface (Barrese et al., 2013a; Fraser and Schwartz, 2012; Kipke et al., 2003; Rousche and Normann, 1998; Simeral et al., 2011; Williams et al., 1999). Among many highly interlinked failure factors, geometry and mechanical mismatches between neural tissues and electrodes play a critical role in the long-term performance of implanted electrodes. Neuronal cells and the cerebral vasculature have sizes on the order of micrometers, whereas neural electrodes are often substantially larger in size. Brain tissues are soft (Young’s modulus in range of kPa), while most conventional neural electrodes are significantly more rigid (Young’s modulus in range of tens of GPa). As a consequence, substantial tissue reactions are typically seen at the interface between brain tissue and implanted device, as manifested by blood brain barrier (BBB) leakage, neuronal degeneration and glial scaring (Kozai et al., 2015b). Furthermore, the tissue’s foreign body reaction also induces a corrosive environment that accelerates the structural degradation of electrodes (Jorfi et al., 2015). As a result, typical recording quality with these electrodes continuously deteriorates over several weeks (A. Gilletti, 2006; Barrese et al., 2013b; P. Rousche, 1992; Subbaroyan et al., 2005; Szarowski et al., 2003). Moreover, their mechanical and structural failures are also often observed sooner than predicted from in vitro tests (Gilgunn et al., 2013; Kozai et al., 2015a; Prasad et al., 2014; Prasad et al., 2012).

It is therefore intuitive to make neural probes with feature sizes that more closely resemble those of their biological host. A number of early studies of conventional electrodes discovered that reducing the diameter of microwires or the width of silicon microelectrodes from 50 – 75 μm to 15 μm induced a significant reduction ($p<0.05$) in neuronal cell death and glial scarring in rodents (Karumbaiah et al., 2013; Schouenborg et al., 2011; Seymour and Kipke, 2007). These studies highlight the importance of electrode geometrical dimension in mitigating tissue reactions and inspired the development of extremely thin neural electrodes. Although it is relatively convenient to micromachine silicon or metal microwires, their mechanical properties make them impractical to use in extremely miniaturized neural probes. More recently, carbon fibers have become a popular choice for

ultra-small (7 μm in diameter) neural electrodes (Kozai et al., 2012) and for constructing arrays (Guitchounts et al., 2013; Massey et al., 2019; Patel et al., 2015). Histological comparisons of tissue reactions to chronically implanted carbon fiber show a significant reduction in foreign body responses than that seen with silicon probes in rodents (Kozai et al., 2012). Carbon nanotube fiber electrodes offer an attractive alternative to carbon fiber electrodes, as they are softer and have a smaller impedance and greater charge injection capacity, making them more suitable for stimulation (Vitale et al., 2015).

Alongside the development of miniaturized intracortical electrodes, increasing efforts have been made to develop flexible neural electrodes (Du et al., 2017; Mercanzini et al., 2008; Sohal et al., 2016; Wu et al., 2015b). There is growing awareness that switching from rigid electrode materials, such as silicon and metals, to softer polymers, such as polyimide and parylene, helps to mitigate tissue reactions and to promote long-term recording stability. However, The Young's modulus of these polymers probes are still $10^6 – 10^7$ larger than that of the brain tissue, and therefore the mechanical mismatch between brain and electrode remains significant. A key issue here is that materials that are as soft as brain tissues typically do not have the necessary properties needed to fabricate functional devices, such as electrical insulation and mechanical strength. This dilemma has been addressed using different approaches. One approach has been to engineer the form factors of the electrodes to achieve a high level of flexibility (Tian et al., 2012). Because most neural electrodes have high-aspect ratio geometries, bending is the dominating deformation that happens at the interface. Therefore, by reducing the bending stiffness of the implanted electrode, deformation forces can be reduced, alleviating the electrode-tissue mismatch. The bending stiffness is estimated by $K_s = E_s wh/12$ for a probe in a slab geometry (Luan et al., 2017), where E_s is the elastic modulus of the material, w is the probe width, and h is the probe thickness. As such, the geometry, in particular the thickness of the electrode, can most efficiently modulate the bending stiffness. A recent series of studies have implemented this concept (Fu et al., 2016; Hong et al., 2018; Liu et al., 2015; Liu et al., 2013; Luan et al., 2018; Luan et al., 2017; Xie et al., 2015) by fabricating neural electrodes at a total thickness of 1 μm, which is ~10 times thinner than previous polymer electrodes. This reduced electrode thickness provided ultra-flexibility and promoted the seamless integration of neural electrodes with host tissue. In vivo imaging of neurons, astrocytes, microvasculature and microcirculation with chronically implanted ultra-flexible electrodes (Luan et al., 2017; Wei et al., 2018), together with postmortem histology (Fu et al., 2016; Xie et al., 2015; Yang et al., 2019), revealed normal neuronal density, an intact blood brain barrier, and little to no glial fibrillary acidic protein (GFAP) responses near the implanted electrodes in rodents. Consistently, these electrodes enabled the stable recording of single-unit action potentials and the tracking of individual neurons for 4 – 6 months (Fu et al., 2016; Luan et al., 2017) without noticeable degradation in recording performance.

Spatial resolution and extent

Intracortical electrodes can only faithfully detect and distinguish nearby neurons (within about 100 μm from the recording site) (Henze et al., 2000). Therefore, in order to record from large populations of neurons that are densely distributed in various 3D anatomical structures, within or across regions, a large array of recording sites need to be implanted in

brain tissues. Inevitably, such a scaling up of recording sites can risk tissue displacement and injury, which need to be minimized. It also raises the challenge of accommodating large-scale, high-density neural electrodes alongside their associated electrical interconnections and mechanical supports, within a small total volume of brain tissue.

Conventional electrodes are impeded by their relatively large physical dimensions, particularly when scaling up channel counts and recording density. For instance, Utah or microwire arrays, which have enabled relatively large-scale recordings (hundreds of neurons) from primates (Dickey et al., 2009; Dotson et al., 2015; Nicolelis et al., 2003; Suner et al., 2005), typically carry only one recording site on the tip of each wire, and usually have contact spacings of >200 μm. They therefore have significant limitations in terms of their recording density and multi-depth coverage. By contrast, microfabricated silicon neural probes carry arrays of electrode contacts that are distributed along the probe shanks, and allow for improved depth coverage (Kipke et al., 2003). These electrodes, however, are also challenging to scale up in density due to the significant tissue displacement and injury they can cause and the total volume they occupy when their current device structure is used to create a high number of recording sites in one host.

Recent efforts to develop high-density neural electrodes have mainly gone in three directions. First, reducing device footprints: this allows for higher-density packing in geometries analogous to microwire arrays. Higher-density microelectrode arrays have been constructed using mechanically strong materials, such as carbon fibers (Patel et al., 2015). These carbon fiber electrodes have diameters as small as 7 μm (Kozai et al., 2012), yet are sufficiently rigid to enable self-supported penetration in a high-density array at an inter-probe separation of 50 – 100 μm. Remarkably, the high-density implantation of carbon-fiber electrodes has induced only mild tissue responses in rodents owing to their ultra-small size (Patel et al., 2015). Polymer-insulated and flexible wire bundles have also been used to generate higher density microelectrodes with a smaller footprint (Guan et al., 2019; Obaid et al., 2020). Second, progress has been made in microfabricating high-density, highly-integrated silicon neural probes (Du et al., 2011; Jun et al., 2017; Rios et al., 2016; Scholvin et al., 2016). This approach takes advantage of advanced fabrication techniques to pattern features on the scale of submicrometer to tens of nanometers. The recording devices are integrated with application-specific integrated circuits (ASIC) to perform signal amplification, band-pass filtering, and multiplexing, enabling neural recording at very high channel counts (of up to 1024 channels). These probes offer a clear advantage in terms of depth-resolved recordings due to the high-density contacts patterned along the longitudinal direction of the probe. However, due to their relatively large dimensions and rigid structures, they typically induce considerable tissue damage, which impedes the high-density implantation of these highly integrated shanks. The third approach involves patterning high-density contact arrays on flexible substrates, to achieve a balance between device dimension and complexity (Chung et al., 2019; Wei et al., 2018). Using this approach, the recording of up to 1024 channels distributed across multiple brain regions has been achieved in rodents (Chung et al., 2019), with minimal tissue responses observed at an inter-probe separation of 60 μm on probes at a footprint of 5 μm^2 (Wei et al., 2018). To facilitate the further scaling up of channel count, these flexible electrodes can be conveniently packaged with high-density amplifiers using standard surface-mount packaging (Musk and Neuralink, 2019). However,

they require rigid shuttle devices for implantation (Hanson et al., 2019; Joo et al., 2019; Zhao et al., 2019), which complicates surgical throughput and adaptation to multiple brain regions and species.

In summary, the need for neural electrodes to: 1) flexibly distribute large numbers of recording sites to target both local and distributed circuits; 2) minimally disrupt the integrity of neural tissue; and 3) track activity across timescales ranging from seconds to months or years, have fueled the exciting development of a variety of novel neural electrodes in recent years. While subsets of these needs have been met by these recent technological advances, as yet no single device meets all of them. The future development of new technologies and the optimization of existing approaches will bring us closer to realizing these goals. Meanwhile, the rapidly growing demand to expand the spatiotemporal scales of neural interface presents significant challenges and opportunities for developing novel transducers, advanced electronics, and signal processing strategies, which we discuss in the following sections.

Power, data, and communication

In order to develop next-generation neural implants for humans and freely behaving animals, advances in electrodes must accompany advances in wireless power and data transfer between the implanted device and a local transmitter/receiver. Conventional power and data transmission rely on a fully wired system with percutaneous wires connected to the neural implant (Fig. 2A). While sufficient in some cases, such as for various types of acute rodent experiments like open field or maze studies, these tethers can become burdensome, limit movement, and open paths for infection, particularly if one desires multiple independent implants (Hargreaves et al., 2004). These challenges have led researchers to look for options to transfer power and data to and from neural implants wirelessly.

While there are many potential solutions to delivering wireless data and power, each consists of three major elements (Fig. 2). (1) A base station (or computer), which processes data and determines the appropriate stimuli to be delivered by the neural implant. (2) A transmitter that is on or near the subject and that communicates with the implant and the base station. (3) The neural implant, which interfaces directly with the target tissue to stimulate or record neural activity. In some small-animal experiments, the transmitter may be too heavy to be worn comfortably by the animal. In such a case, the transmitter can broadcast over an arena in which animals can freely move and behave (Fig. 2B). This type of system is often ideal for rodent studies that involve their interacting with objects or for chronic experiments. For example, this approach allowed rodents to move through tubes that would have been impractical using a fully wired system (Singer et al., 2020), as well as the recording of long-term measurements compatible with home cage transmitter setups (Montgomery et al., 2015; Shin et al., 2017). In the case of large animals and humans, this relay might consist of a wearable electronic element (Fig. 2C), such as a mid-field powered wireless system (Agrawal et al., 2017).

While the link between the base station and transmitter may be wired, or supported by mature wireless technologies such as WiFi or Bluetooth, a significant challenge for next-

generation implants is the link between the transmitter and the implant. This data and power link must operate through tissue and bone and, in some cases, it must communicate with millimeter-sized devices that cannot support traditional electromagnetic antennas. Here, we describe three general designs for a wireless system and the performance tradeoffs that come with the different wireless communication techniques (Fig. 2D). We have categorized these wireless data communication and power transfer techniques as “Electromagnetic”, “Magnetic”, or “Acoustic”; however, some techniques consist of mixed modalities and thus could fall into multiple categories. One example is near field inductive coupling (NIC), which we consider here as a magnetic technique because it is powered using a magnetic field; however, NIC can also be considered to be an electromagnetic technique given that the implant’s current is driven by an electromotive force. As a result, the reader may find these techniques classified differently in other work based on the authors’ preference.

Electromagnetic Techniques:

Radio frequency signals (RF, ~2.4 GHz) are a kind of far-field electromagnetic waves that implanted electromagnetic antennas use to transfer power and data to and from a transmitter. In these systems, the implant will usually include a metal trace that is ~3 cm long in order operate at resonance where the device can absorb the most power from the electromagentic wave (1/4 of the wavelength of the 2.4 GHz singal). One can create smaller antennas (Khalifa et al., 2019; Rahmani and Babakhani, 2017), but these compact designs typically do not resonate with the RF wave, which results in reduced efficiencies and are more challenging to design. As a result, the relatively large wavelength of RF signals is the primary factor that limits device miniaturization. Despite this potential drawback, bi-directional RF communication is relatively easy to implement because much of the equipment and full research systems are available from commercial vendors. Another advantage of this type of system is that RF works well when traveling through air, which does not absorb electric or magnetic fields, meaning the transmitter does not need to be in direct contact with the skin. Due of this, RF has applications in freely moving rodent studies, such as home cage or open field experiments (Park et al., 2016b). However, RF is absorbed in tissue and can cause damage if it exceeds safety limits, it is a good candidate for powering shallow implants. Indeed, many RF implants are < 1 cm deep and located just beneath the skin. In some cases, they may be wired to power more deeply implanted electrodes (Park et al., 2016b).

Visible and near infrared light (~300-650 THz) is also used for_bi-directional communication and power in miniature implants (Cortese et al., 2020). In such devices, silicon photovoltaics, which capture input light and transform it to electrical current, provide power to the device while a microLED communicates an output light signal. Light scattering in tissue, where incident light is “scattered” away in various directions as it interacts with tissue, limits these implants to shallow regions, again generally just beneath the skin. While the power delivered by such implants is low relative to other techniques (typically 60 μW or lower), they can be made to be exceptionally small (8 μm × 75 μm × 175 μm). As a result, optical links are a good candidate for surface or tethered implant applications where other types of wireless implants would be too large. For example, researchers have used these

miniature prototypes as an implantable temperature sensor in mice (Cortese et al., 2020) and have proposed a system that would record neural activity (Lee et al., 2018b).

Midfield electromagnetic waves (MDF, 1.6 GHz) offer yet another option_to deliver energy to miniature implanted coils wirelessly in rodents and large animals (Agrawal et al., 2017; Montgomery et al., 2015). At MDF operating frequency, the electric component of an electromagnetic wave is engineered to couple into tissue, allowing for deeper tissue penetration (up to 4.5 cm deep has been demonstrated in a porcine animal model), at safe RF exposure levels (Agrawal et al., 2017). This prototype method can also be used to power shallow (below-skin) rodent implants over a behavioral area (Montgomery et al., 2015). The magnetic component is absorbed by the implanted coil to inductively power the electronics. Due to the safety limits that restrict the amount of energy the transmitter can deliver to the tissue, the received power is typically limited to a maximum of about 1 mW. Due to tissue absorption, the received power decreases further when the implant is placed deeper into the tissue. While this method has yet to demonstrate the transfer of data back to the transducer, it remains a good candidate wireless data and power transfer technology for low-power implants that are millimeters to centimeters below the surface of the skin.

Magnetic Techniques:

Near field inductive coupling (NIC) is another commonly used wireless power system that has commercial systems and equipment available for it and that can support bi-directional communication. This traditional technique uses alternating magnetic fields (usually 13 MHz) delivered to an implanted resonant inductive coil. The implant captures the magnetic flux and induces a current in the coil. The resonant frequency of these implants is tuned based on the inductance of the coil and an onboard capacitor. Magnetic fields at these frequencies suffer little absorption in tissue; however, the power the implant can gather depends upon the coil area and alignment with the transducer. As a result, most bioelectronic applications require a larger coil, >1 cm in diameter, to receive adequate power transfer. In a prototype inductive system that operates a rodent implant over a behavioral area (Shin et al., 2017), the implant was approximately 1 cm in diameter, implanted just below the skin, and able to receive 8 mW of power. In small animals, pickup coils of this size typically cannot be implanted deep in the animal; however, large animals and humans can often support deep implantation of cm-sized devices, depending on the target area. Similar to RF, NIC technology is generally a suitable choice for shallow or tethered implants. However, one of the major advantages of NIC is that increasing the size or number of turns in the pickup coli will increase the received power. As a result, devices that are cm-scale and larger are often most efficiently powered by NIC.

Magnetoelectric wireless power transfer (ME, 250-400 kHz) also uses magnetic fields to deliver power to a miniature implant (Nan et al., 2017; Singer et al., 2020; Yu et al., 2020a). The implant combines a magnetostrictive and a piezoelectric material. An alternating magnetic field applied to the magnetostrictive component generates stress within the device, which is transferred to the piezoelectric element and converted to an electrical signal used to power an implant. These implants have acoustic resonant frequencies, which allows for miniature resonant devices. For example, a prototype implant in a freely moving rat

delivered up to 2 mW of power to a mm-scale device implanted under the skin (Singer et al., 2020). Yu et al. further developed this technique and created an 8.2 mm^3-sized neural stimulator that also used ME to receive digital data (Yu et al., 2020a). However, data transmission from the implant back to the receiver has yet to be demonstrated using ME techniques. As a result, the current ME methods are best applied to devices with on-board data storage, such as neural stimulators or recorders, where the ability to transmit data from the implant to the base station is not a major design requirement. Compared to NIC, ME techniques typically have higher power densities when devices are made small. As a result, ME data and power transfer are particularly attractive for mm-sized devices that operate at mW levels deep below skin and bone.

Acoustic Techniques:

Ultrasound (US, 1.85 MHz), has also emerged as an alternative for wireless power transfer using safe levels (692 mW cm^{-2}) of pressure waves to deliver power to a small implanted piezoelectric crystal (Piech et al., 2020; Seo et al., 2016). The piezoelectric absorbs the pressure waves and transduces them to electrical energy, which is harvested and used to power low-power electronics. These piezoelectric crystals are small because they naturally vibrate at wavelengths that are smaller than electromagnetic waves of the same frequency. Recent demonstrations have shown, a 1.77 mm^3 US powered neural stimulator delivers up to ~1 mW of power (Piech et al., 2020)). Notably, US can also be used to transfer data back to the transducer using the reflection of ultrasound waves that travel back to the ultrasound transmitter/receiver. This bi-directional communication has been demonstrated with a 2.4 mm^3 device on rodent sciatic nerve (Seo et al., 2016). One potential drawback for US data and power transfer is the fact that the transducer must be in direct contact with the body using impedance matching gels or foams. While miniature US transducers can be carried by rats (Lee et al., 2018c), the size and weight may be impractical for mice and for many experiments that involve freely behaving small animals. Additionally, acoustic reflection at the tissue bone interface can decrease data and power transfer through the skull, leading to the proposal for subdural US transducer arrays (Seo et al., 2015). Despite these potential limitations, US has emerged as a promising wireless power and data transfer method for next-generation simulation and recording devices, particularly for humans and large animals.

The use and combination of these different power-transfer techniques lead to three general classes of wireless implants with different degrees of invasiveness (Fig. 3): 1) A shallow wireless link (through skin) between a transmitter on the scalp and a receiver below the skin that is wired to a cortical or sub-cortical device; 2) a deep wireless link to subcortical s via a relay implanted beneath the skull; and 3) a deep wireless link (through skin and skull) directly between a transmitter on the scalp and subcortical implant. In the first case (Fig. 3A), all the wireless data and power transfer techniques perform well over short distances. In particular, RF, NIC, and light, are well suited because tissue absorption is not a major concern for this configuration. This setup is also commonly used in rodent neural implants where brain regions are too small to implant power-harvesting devices into the tissue directly.

The second case (Fig. 3B) consists of secondary implanted relay channels and transmits power wirelessly to distributed device(s) that are too deep, too small, or too numerous to be wired directly to a cortical receiver. This relay system also allows for multiple modes of wireless power to be used in one application, where a single relay station can communicate individually with multiple small optical or ultrasound devices (Lim et al., 2020; Seo et al., 2016).

The third case (Fig. 3C) consists of a deeply implanted small device that can be activated directly from the external transducer. Devices such as these generally use MDF or ME power transfer techniques. They will likely see many future applications for minimally invasive deep implants in larger animals, when devices must be small and implanted relays are impractical or undesirable.

In the future, new hybrid implants that combine different modes of power transfer could enable wireless closed-loop implants to be generated that could stimulate and record neural activity deep in the brain. (Fig. 3D) Furthermore, new techniques to reduce the power required at the implant and to reduce the footprint of the required electronics will also lead to smaller, less invasive bioelectronics for all power transfer techniques. Ultimately, the choice for the best wireless data and power delivery system will likely come down to a choice between performance and invasiveness under specific experimental constraints. For example, the implant depth, size, and power requirements, along with the ability to perform a large craniotomy and to maintain contact between the external transmitter and the implant, will all factor into the decision about which technology to use for a given application.

Electronics for neural interfaces

The electronics part of a bidirectional neural interface bridges the gap between the neural implant and the computer. A typical implementation consists of five major building blocks (Fig. 4), namely amplifier, filter, analog-to-digital converter (ADC), stimulator, and communication interface. The rationale behind this architecture is explained as follows. First, typical neuronal signals are weak, ranging in amplitude from tens of μV to several mV, and thus require sufficient amplification with low noise. Second, depending on the specific frequency ranges of interest, i.e., field potentials (<1 Hz to 300 Hz) or action potentials (300 Hz to 10 kHz), spectral filtering is often necessary to reject interferences and noise outside the desired frequency band. Third, since computers can only process and store information in the digitalized format as a series of ones and zeros, ADC is used to convert the analog neuronal waveforms into binary digital streams. Fourth, neurons can be electrically stimulated using current or voltage pulses, which are generated by a programmable stimulator in the stimulation path. Finally, the bidirectional communication interface sends the recording data to a computer for signal processing and decodes the commands from the computer to program the chip. The discussion in this section focuses on integrated neural recording/stimulation chips rather than discrete instrumentation circuitries. Since integrated electronics combine all the necessary building blocks into a single silicon chip, they offer a much smaller footprint and lower cost and can be directly packaged with neural implants as a wearable device for longitudinal experiments.

Depending on the application, the goals of neural interface design and in turn the electronic design fall under two major categories. 1) Applications such as brain-machine interfaces (BMI) necessitate a high channel count and fine spatial-temporal resolution to enable large-scale and high-density monitoring of neural activities. In these applications, the design emphasis has been on lowering down the power consumption and area of the electronics to enable battery-powered wearable devices while maintaining a high signal fidelity. 2) On the other hand, miniaturized neural implants for recording and stimulation of a small region of the central or peripheral nervous systems typically require much fewer channels compared to a BMI, but prefer untethered operation. The key design focus there is to integrate wireless data/power transfer into the device.

Integrated Electronics for High-Channel-Count Interfaces.

The first design of integrated neural recording amplifiers packaged with a microelectrode array was presented in 1971 (Wise and Angell, 1971). Since then, significant research progress has been made in integrated neural electronics to increase the number of parallel channels while maintaining low power consumption, noise, and size. State-of-the-art *in-vivo* neural recording chips can monitor up to approximately a thousand parallel channels with ~50 μW averaged dc power per channel (Mora Lopez et al., 2017; Musk and Neuralink, 2019; Park et al., 2018; Shulyzki et al., 2015). On the other hand, although not designed for *in-vivo* applications, several *in-vitro* neural recording chips have demonstrated parallel recording with more than 1,000 channels. In 2017, Dragas et al. presented a high-density neural recording chip that enables simultaneous recording of 2,048 channels out of 59,760 on-chip microelectrodes (Dragas et al., 2017). While the co-integration of $3 \times 7.5\ \mu m^2$ on-chip microelectrodes and off-chip implanted neural probes present a significant challenge for packaging (Obaid et al., 2020), the rest of on-chip circuitry achieves a similar electrical performance compared to chips designed for *in-vivo* applications and can be potentially scaled up to construct an *in-vivo* recording/stimulation chip with several thousand channels.

Remarkably, the electrical performance of state-of-the-art neural recording chips is comparable to that of commercially available benchtop electrophysiology signal acquisition systems. From a user's perspective, the selection of which chip to include or emulate in the interface design mainly depends on the targeted neuroscience application and in turn the requirements of channel counts, power budget, and the packaging scheme. To better benchmark the electrical performance of neural recording chips from a system designer's perspective, two figures of merits are proposed in (Park et al., 2018). The first figure of merit, called Channel FoM, is defined as

$$\text{Channel FoM} = \frac{P_{\text{Ch}}}{2^N \cdot f_S}$$

where P_{Ch} is the averaged power consumption per channel, N is the effective number of bits of the digitized output, and f_S is the ADC sampling rate. f_S is typically set as twice that of the highest frequency content of interest, e.g., 20 kHz for recording action potentials. With a fixed sampling rate f_S, a lower Channel FoM indicates better energy efficiency and lower noise. The second figure of merit, called Energy-Area FoM (Park et al., 2018), includes

channel area into comparison, which is an essential design parameter for wearable BMI and directly affects the chip fabrication cost. It is defined as

$$\text{Energy-Area FoM} = \frac{P_{\text{Ch}} \cdot A_{\text{Ch}}}{2^N \cdot f_S} = \text{Channel FoM} \cdot A_{\text{Ch}}$$

where A_{Ch} is the averaged area per channel. Fig. 5 summarizes the milestones of recently reported neural recording chips and indicates the desired technology direction to further improve the energy efficiency, area efficiency, and signal fidelity.

Electronics for Miniature Neural Implants.

Significant progress has been made in the last decade in miniaturizing wireless neural implants to stimulate and record neural activity in addition to revolutions in wireless data and power transfer technologies (discussed in Section 2), advances in system and circuit designs drive the creation of smaller yet more capable neural implants. Here we discuss specific system design challenges and solutions in miniaturizing wireless and implantable interfaces for neural stimulation and recording.

Regardless of the modality of interface (electrical, optical, etc.), the core functionality of stimulation implants is to perform well-controlled stimulation based on wireless commands. A range of mechanisms has been developed to perform this task, ranging from simple, analog controls with a few components to complex, digital systems that consist of thousands of transistors (Fig. 6). These approaches achieve different trade-offs in device size, complexity, controllability, and stability. By directly modulating the wireless carrier waveforms with the desired stimulation pattern, the simplest and smallest implementation of wireless stimulator can be achieved. The carrier waveform is sinusoidal if the wireless modality is electromagnetics or ultrasonics. Otherwise, it will be a constant direct signal. The implant recovers the stimulation waveform in real time with simple rectifier circuitry, which extracts the amplitude of modulated waveforms (Fig. 6A). Examples of such neurostimulators include: a 0.5-mm^3 inductively powered and amplitude shift-triggered electrical stimulator (Freeman et al., 2017); a 0.01-mm^3 optically powered and pulse-triggered electrical stimulator (Seymour et al., 2014); a 0.009-mm^3 radio frequency-powered and pulse-triggered electrical stimulator (Khalifa et al., 2019); and nm-scale magnetothermal nanoparticles (Chen et al., 2015). The main drawbacks of this miniaturization approach is that it leads to signal variability and achieves lower stimulation power. Wirelessly transferred signal varies significantly *in vivo* due to relative distance and alignment between the transmitter and receiver, and physical properties of different mediums. These variations will lead to inconsistent and unpredictable stimulation waveforms. Moreover, the lack of temporary energy buffer, like a capacitor, in this scheme significantly limits the achievable stimulation power. One of the highest reported power was 55.5 μW (Seymour et al., 2014).

To address these challenges, a number of recent implantable neurostimulators employ integrated circuits to regulate power and data transmission. The wireless signal to the implants still carries stimulation information, but in the form of modulated digital bits. The digital data is then decoded at the implant to program the stimulation amplitudes and pulse

widths (Fig. 6B). Neurostimulators that utilize such a mechanism include: a 9.375-mm^3 inductively powered 1-mW optical stimulator (Jia et al., 2019); a 8.2-mm^3 magnetoelectrically powered 0.24-mW biphasic electrical stimulator (Yu et al., 2020b); and a 1.7-mm^3 ultrasonically powered 0.12-mW monophasic electrical stimulator (Piech et al., 2020). When real-time control of a large number of electrodes is desired, a recent study has shown the potential of completely embedding imaging sensors, signal processors on a 17.25-mm^2 silicon chip to program stimulation for a retinal prosthesis (Fig. 6C), which circumvents the wireless communication bandwidth and power bottlenecks (Park et al., 2020b) (Fig. 6D).

Many neural implants are also designed to record and wirelessly transmit neural activity out of the body to receivers (RX). The simplest, effective neural recorder was demonstrated with a single transistor and ultrasonic transducer, which leverages low-power backscattering technology to transmit captured neural signals (Seo et al., 2016). In backscattering, the implant modulates the amplitude of incoming acoustic carrier waves generated by an external transmitter (TX) with neural signals and reflect the waves (Fig. 6E). Digitization of neural signals is pushed to external RX with much relaxed power budget. Because the implant does not generate the carrier waves, its power usage is minimized. However, the absence of a low-noise amplifier limits the fidelity of the recorded signal and restricts the tissue operation depth range to less than 8.8 mm. In order to address these challenges, sub-mm sized and ultra-low-power integrated circuits have been developed to perform low-noise neural signal amplification. A 250 μm by 57 μm opto-electronically transduced mote employs such an integrated circuit to amplify neural signals and perform less noise sensitive pulse position modulation of light for data upload, which shows a working depth of around 6 mm limited by tissue attenuation (Lee et al., 2018a). A 0.8 mm^3 ultrasonically transduced mote further extends the depth to 50 mm and enables multi-mote recording through orthogonal subcarrier modulation (Ghanbari et al., 2019). A major limitation of this type of neural signal backscattering devices is that only one recording channel can be recorded and transferred in each device. To support multi-channels, the amplified neural signals need to be digitized by ADCs and transmitted with digital communication technologies (Fig. 6F). A 2.5-mm^3 16-channel electro-cortical interface was demonstrated recently with this architecture (Ha et al., 2017). The introduction of ADCs not only increases the number of recording channels, it also largely avoids noise added during wireless communication by leveraging noise tolerant digital communication technologies. Further, digitized neural signals enables in-situ signal processing with energy-efficient integrated circuits and sending out extracted features instead of the complete recordings (Fig. 6G), which promises orders of magnitude reduction of wireless data rate and power consumption. A recent 1-mm^3 single-unit activity recorder demonstrates the feasibility of such a system (Yeon et al., 2018). Despite the many benefits provided by digitizing recorded signals, ADCs come with high power consumption, dominating the total power of a neural recording implant. A recent study explores the possibility of performing signal processing directly in the analog domain before digitizing, which shows a 190 μm by 170 μm integrated circuit capable of extracting spiking frequency bands with 920 times lower power than digital counterparts (Lim et al., 2020). On-chip signal processing and feature extraction also enables the potential for autonomous closed-loop neural modulators. (Fig. 6H)

In summary, design optimization of (integrated) electronics to approach the system goals (e.g. high channel count or miniaturization) of the implant and its integration into the neural interface are critical to the success of the device, both for recording and stimulation at the point of interest.

Bi-modal electrical-optical neural interfaces

Electrophysiological and optical imaging techniques have complementary strengths in spatiotemporal resolution and coverage (Fig. 7A). Optical imaging techniques such as wide-field and multi-photon calcium imaging (Guo et al., 2014; Helmchen and Denk, 2005; Stosiek et al., 2003) have become extremely powerful in resolving neural activity over large-scale networks. They, however, only provides an approximate reflection of spiking and have time constants typically ≥100 ms (Chen et al., 2013), which is often too slow to resolve neural dynamics on the time scales of milliseconds. Voltage imaging (Peterka et al., 2011) may obviate these problems and can measure sub-thresholds events in local activity (Abdelfattah et al., 2019; Adam et al., 2019). They, however, appear to confront limitations in sensitivity and labelling density for mapping neural network at a larger scale. In contrast, electrophysiological measurements have very high temporal resolution, and can record the precise timing of individual action potentials. However, cell-type and cell-projection specificity are harder, if not impossible, to achieve when using electrophysiological measurements. Therefore, combining electrical and optical imaging modalities in the same brain leverages their complementary strengths and provides a promising approach for monitoring large-scale network activity simultaneously with the activity of local neural populations at high spatiotemporal resolutions.

There are, however, a few challenges to address when it comes to integrating electrical and optical measurements for *in vivo* brain studies. First, optical excitation generates laser-induced photoelectric artefacts in metallic electrodes that interfere with electrophysiological measurements (Kozai and Vazquez, 2015). Multiple photoactivation modes, such as the photovoltaic (Becquerel effect) and the photothermal effect, appear as transients or oscillations in recordings that interfere with local field potentials (LFP) or single-unit spiking activity, depending on the frequency and duration of the light stimulus. Furthermore, conventional neural electrodes are oblique, rigid and optically opaque, which are ill-suited for simultaneous optical measurements. Their implantation often imposes constraints on the accessibility of the field of view and/or on the placement of an imaging microscope objective (Poskanzer and Yuste, 2016).

Simultaneous electrical and optical recordings

Recent technological developments have provided valuable solutions to the aforementioned challenges (Fig. 7B). First, because the artefacts from the photoelectric effect are dependent on the laser-scanning rate at a fixed fequency spectrum and are often present at multiple electrodes simultaneously, such artefacts can be attenuated by post-processing, for example, by imposing digital bandstop filters (Shew et al., 2010) or common mode referencing (Ludwig et al., 2009). Furthermore, the use of graphene as a novel electrode and interconnect material has eliminated photoelectric artifacts, offering artefact-free

electrophysiology in combination with optical imaging and stimulation on tissue slices (Kuzum et al., 2014), on the brain surface (Park et al., 2016a) and deep in the brain in rodents (Thunemann et al., 2018). Additionally, graphene is optically transparent, which, when fabricated on a transparent substrate such as parylene C, avoids light attenuation when transmitting through the electrode and the subsequent shadow effect. Other novel materials, such as ZnO (Lee et al., 2015), carbon nanotube web-like thin films (Zhang et al., 2018), and transparent organic transistors (Benfenati et al., 2013; Lee et al., 2017), have also been successfully used to construct neural electrodes for concurrent optical imaging. Lastly, the emerging emphasis on the flexiblility of neural electrodes provides a viable solution to the geometrical contraints that exist between optical and electrical modalities. These flexible probes bend without breaking. For example, ultraflexible electrodes at a total thickness of 1 μm can bend at a radii of curvature of < 100 μm (Luan et al., 2017). This permits one or more devices to be inserted underneath or through small hole(s) in an imaging window and then bent out of the way without interfering with cranial optical window implantation or with the placement of microscope objectives.

Owing to the versality of optical methods, these flexible and transparent electrodes have also been used alongside various imaging modalities, such as laser speckle contrast imaging of cerebral blood flow (Luan et al., 2018) and optical coherence tomography of micro-vasculature (Park et al., 2016a). Such combinations enable the simultanenous monitoring of multifaceted brain activity, such as neurovascular coupling (He et al., 2020). In vivo imaging is also useful in the development and optimization of electrode technologies by enabling the tissue-electrode interface to be visualized. For example, the longitudinal two-photon (2P) imaging of neurons, microvasculature and astrocytes surrounding implanted ultraflexible electrodes has shown that tissue damage caused by implant surgery recovered over a period of a few weeks, and that there was an intact blood-brain barrier and no chronic neuronal degradation nor glial scarring (Luan et al., 2017). 2P calcium imaging before, during, and after electrode implantation has also shown that rigid electrode implantation leads to prolonged, elevated calcium levels in neurons within 150 μm of the electrode interface that is related to mechanical trauma (Eles et al., 2018). 2P imaging of microvasculature has also been used to determine brain compression and tissue damage during device implantation as a function of the device’s form factors (Melosh, 2019).

Optical stimulation with electrical recordings

A powerful optical approach to deciphering functional neural connectivity is optogenetics (Boyden et al., 2005). Exciting advances have generated genetic tools that can be used to precisely manipulate individual neurons and specific cell types, and these tools have fuelled the demand for devices that can simultaneously perform electrophysiological recordings and optical excitation. Because the visible light needed for opsin activation is scattered and absorbed by neural tissue, optogenetic neuromodulation relies on implanted devices that can deliver optical stimuli deep into the tissue. Early approaches centered on constructing or packaging passive optical waveguides onto mature neural recording devices, such as Utah arrays, Michigan probes, tetrodes and microwires, which previous review articles have summerized (Chen et al., 2017). More recent technologies have focussed on suppressing the stimulation artefact, accomodating more functionalities, and on providing flexible and

minituarized form factors, as well as scalibiity in fabrication. Most of the transparent electrodes discussed above provide artefact-free electrical recording concurrently with optical stimulation (Kuzum et al., 2014; Lee et al., 2015; Park et al., 2016a; Thunemann et al., 2018). The monolithic fabrication of μLEDs and their integration with Michigan probes has been used to provide 12 μLEDs on each 32-channel shank. The resulting probe has enabled depth-defined recording and channelrhodopsin (ChR2)-mediated optogenetic stimulation in the rat hippocampus (Wu et al., 2015a). A similarly scalable method was developed further to fabricate high-density, flexible optoelectronic neural probes with embedded μLED to improve the tissue-probe interface (Reddy et al., 2019). In addition, thermal drawing, which is commonly used in optical fiber production, has recently enabled the straightforward and cost-effective integration of polymer optical waveguides with conductive electrodes made of low-melting-temperature metals (Canales et al., 2015) or of polymer composite (Park et al., 2017). The diameters of these multifunctional probes was as small as 70 μm, leading to considerably less glial response and to less damage to the blood brain barrier after implantation (Canales et al., 2015). Further optimization of the design and fabrication process of these multifuctional probes have enabled one-step fabrication (Park et al., 2017) and minimal photoelectric effects that permited continuous light stimulation at low frequency during recording (Kilias et al., 2018). Lastly, an alternative approach to construct multifunctional probes was realized by conformally attaching ultralflexible electrode arrays onto conventional optical fibers. Because the ultra-thin coating devices were fabricated separately using planar photolithography, high resolution and high throughput can be achieved without being limited by the geometry and materials of the optical waveguide (Zhao et al., 2017).

Taken together, these exciting developments in device technologies and in the methodologies used to integrate neural recording with optical modalities have greatly expanded the spatiotemporal resolution and coverage of these devices, and thus our ability to map and manipulate brain functions. Furthermore, many of these devices can be adapted to accommodate additional modalities to measure and control the brain’s chemical activity, such as electrochemical sensing through functional materials on flexible (Fan et al., 2020) or rigid (Taylor et al., 2019) electrodes, and the in vivo delivery of neurotransmitters through multifunctional fibers (Park et al., 2020a). These integrated approaches will open up new opportunities to elucidate the links between the electrical and chemical activity in healthy and diseased brains.

From signals to key features: neural data processing

The broadband signals acquired by neural interfaces generally contain two types of voltage signals. The high-frequency spikes (300 Hz to 10 kHz) are the extracellular action potentials generated by individual neurons as measured by intracortical microelectrodes, and the low-frequency field potentials (<1 Hz to 300 Hz), derive from a population of neurons in a small volume of tissue. In this section, we review recent progress in spike sorting – the process of detecting spiking events and assigning different spike waveforms to putative single neurons (Gold et al., 2006) – and in extracting features from low-frequency extracellular field potentials (Fig. 8). Prior to analyses, the neural signals often undergo pre-processing to ensure that the signals do not covary due to non-biological confounds, such as electrical

cross-coupling, line noise, or the artificial splitting of neuronal responses in recording, which can lead to fallacious inferences. The pre-processing typically uses one or a combination of the following schemes: whitening, common average referencing, surface Laplacian transform, and Independent Component Analysis (ICA) (Whitmore and Lin, 2016).

Spike detection and classification.

Spike sorting typically consists of a sequence of steps, including band-pass filtering the data, detection of threshold-crossing events, feature extraction of the spike shapes, and clustering of the waveforms (Lewicki, 1998). Classical spike sorting algorithms were designed to work with a small number of electrodes (typically a few tens of electrodes). However, these algorithms suffer from substantial limitations when they are used to process neural data generated from higher density electrode arrays with a much larger channel-count, for several reasons. First, many algorithms do not take into account that a single neuron will evoke spikes on many (tens of) electrodes. The automated clustering process in these algorithms, while working well at low dimensions, often performs poorly as the dimension of the analyzed data increases, an effect termed as the ‘curse of dimensionality’ (Rossant et al., 2016). Second, previous algorithms require substantial manual processing, such as curating the results by selecting which clusters to split, merge or reject (Einevoll et al., 2012). The manual process, while manageable with low-count probes, cannot scale up to hundreds and thousands or more channels. Third, the resolution of spatiotemporally overlapping spikes becomes both more tractable and more important with more channels and with higher contact density, which is not sufficiently considered in these algorithms.

Multiple algorithms and systems have been developed to meet these needs for spike sorting of high-channel count, high-density electrode data. To resolve the problem of temporally overlapping spikes, KlustaKwik algorithm detects spikes as spatiotemporally connected events based on the prior knowledge of the probe geometry (Rossant et al., 2016). It uses a dualthreshold (weak and strong) approach to allow areas joined by weak threshold crossings to be merged and to avoid spurious detection of small-noise events. When assigning spikes to neurons, it employs a mask vector in addition to a feature vector in principal component analysis (PCA), which allows temporally overlapping spikes to be clustered as coming from separate cells (Rossant et al., 2016). Kilosort (Pachitariu et al., 2016), an open-source software suite, takes advantage of a novel mathematical approach that omits spike detection and PCA and instead combines the identification of template waveforms and associated spike times in a single unified model. This approach, together with the computing capabilities of low-cost commercially available graphics processing units (GPUs), greatly reduces the amount of calculation required and accurately sorts spikes from the output of 384-channel dense probes in approximately real time. SpyKing Circus (Yger et al., 2018) can process recordings from thousands of electrodes with high sorting accuracy and real time performance. The algorithm parallelizes density-based clustering to find the centroid of each cluster rather than the border. It is combined with template matching to deconvolve overlapping spikes in a computationally efficient manner to eliminate multi-unit activity during clustering. MountainSort (Chung et al., 2017), another fully automated open-source approach to spike sorting, uses an efficient, nonparametric, density-based clustering

algorithm termed ISO-SPLIT in a low-dimensional feature space of the spike events. The processing time scales linearly with the number of electrodes. Using multiple processors with hyper-threading capability, it can cluster a 128-channel dataset much faster than real time (Chung et al., 2017).

These novel, automating spike-sorting algorithms provide substantial advantages over earlier methods, eliminating the need for manual curation, and improving processing efficacy and accuracy. The on-going effort to further develop these approaches is focused on addressing two remaining challenges: overlapping spikes and drift. Kilosort2 improves on Kilosort primarily by employing drift correction, which changes the templates continuously as a function of drift (Pachitariu et al., 2019). While these algorithms successfully resolve coincident spiking events where the two neurons are sufficiently separated in space, they cannot yet resolve spike waveforms that significantly overlap on the same electrode. Model-based frameworks for post-sorting corrections may might be a viable approach to identifying these events (Chung et al., 2017).

Lastly, but importantly, depending on the user-specific goal or the question to be answered, spike sorting can be altogether skipped instead employing multi-unit threshold crossings to estimate low-dimensional neural population dynamics (Deng et al., 2015; Trautmann et al., 2019). This is particularly applicable when the multiunit recording channels substantially outnumber the dimension of the underlying neural activity (Trautmann et al., 2019). These findings provide a scientific rationale for relaxing the requirement on the sampling rate, storage, processing, communication bandwidth, and power, and enable large-scale electrophysiology in applications where these factors constrain the number of channels.

Feature extraction from field potentials.

Extracellular field potentials (Buzsáki et al., 2012; Pesaran et al., 2018) reflect activity of a population of neurons, and are referred to as electroencephalograms (EEG) when measured at the scalp, electrocorticogram (ECoG) when recorded with subdural grid electrodes, and as local field potentials (LFP) when using invasive depth, micro or thin-film electrodes. The magnetic field induced by the same activity is measured by the magnetoencephalogram (MEG). All field potential recordings have millisecond temporal precision, although they differ in their spatial coverage, resolution and degree of invasiveness.

The LFP is a promising signal for steering neuroprosthetic devices (Einevoll et al., 2013), brain-machine interfaces (Andersen et al., 2004) as it is more stably recorded in a chronic setting than spikes. The growing development of large-scale, high-density electrodes (Chung et al., 2019; Csicsvari et al., 2003; Khodagholy et al., 2015) greatly expands the possible functionality that can be achieved from these devices. Several studies have used LFP to investigate cortical mechanisms in motor planning (Scherberger et al., 2005), sensory and higher cognitive processing (Belitski et al., 2008; Kreiman et al., 2006; Pesaran et al., 2002), and seizure detection and prediction (Brunton et al., 2016; Erfanian and Aazhang, 2019). However, the LFP signal is inherently ambiguous due to contributions from multiple sources (Kajikawa and Schroeder, 2011; Lindén et al., 2011; Mukamel et al., 2005), like synaptic potentials, somatic action potentials (spikes) and from distant sources due to volume conduction, making them harder to interpret than spikes. Spikes are mostly an extracellular

aggregate of membrane potentials largely measured at the soma. This can be resolved by the development of appropriate mathematical models and computational tools based on experimental validations and measurements (Brown et al., 2004; Stevenson and Kording, 2011) to disentangle local activity from remote sources. Some of the state-of-the-art data-processing methodologies for LFP recordings are summarized below.

Local signals and their changes with experimental conditions are often assessed by decomposing them into their constituent frequencies and performing spectral analyses. Power density, which gives the distribution of energy with frequency and autocorrelation, which finds repeated patterns in the time-series, are some of the analytical techniques used. An assumption of these estimates is that neural activity is stationary, i.e. the properties of the signal do not change with time, which is often unrealistic with transient events, such as around stimulus onset, or even in the absence of sensory inputs (Einevoll et al., 2013; Pesaran et al., 2018). Spectral estimates can be computed for periods when the signal is locally stationary. The spectra of LFPs can also detect oscillatory events in the brain, such as gamma and theta oscillations. Changes in spectral power within certain frequency ranges can arise from an increase in the number of active neurons or to an increase in temporally synchronous activity without increase in active neuronal numbers. Oscillatory events that do not shape the spectrum can sometimes be detected with a peak in spike-field coherence (SFC) – a measure of phase synchronization between the LFP signal and spike times as a function of frequency (Buzsáki et al., 2012; Pesaran et al., 2018). Changes in SFC have been associated with certain cognitive or perceptual tasks (Chen et al., 2015a).

To capture dependencies between neuronal signals, linear measures, such as cross-correlations and coherency measures, are often used to capture correlated patterns of activity, using locally stationary time intervals. A critical confounding factor in this approach is that both measures are influenced by the signal-to-noise ratio. To investigate causal inferences with directionality among brain regions, Granger Causality (GC) is a well understood and widely used method (Barnett and Seth, 2014). GC is a statistical hypothesis test for determining whether one time-series has information to forecast another time-series. However, the primary concern when using GC is potential model mismatch, since the measure depends on parametric models. Nonparametric estimates are preferred as they have improved bias and variance properties. Recently, information theoretic tools, such as Directed Information (DI) and Transfer Entropy (TE) (Amblard and Michel, 2013), have gained prominence in neuroscience due to their applicability to a wide range of neural recordings (spikes and field potentials) (Cai et al., 2017; Malladi et al., 2016), without model assumptions. While a larger number of samples are required to estimate such directional causality compared to GC, recent developments in information theoretic estimation using the nearest neighbor approach (Gao et al., 2015) and deep learning (Gabrié et al., 2018) have greatly improved the accuracy of these tools, even when using lower sample regimes.

Another basic question is whether LFPs reflect local activity or that of remote sources. Because different neuronal activities could generate the same field potentials (Pesaran et al., 2018), it is not possible to interpret field potentials as a sum of their cellular sources. However, using LFPs from invasive, high-density electrodes, current-source density (CSD) analysis can reveal sources and sinks that contribute to the LFPs. Spurious inferences can be

avoided by making field potential measurements in all three spatial directions, or by using prior constraints and assumptions (Potworowski et al., 2012) The estimation of the density of trans-membrane current sources (CSD) generating the LFP can help localize synaptic dynamics.

The parallel multi-region recording of neuronal activity promises to improve our understanding of the neuronal representation and storage of information (Brown et al., 2004; Stevenson and Kording, 2011). With multiple recordings, dimensionality reduction techniques, such as Gaussian process factor analysis (GPFA) and state-space methods (Cunningham and Byron, 2014), have been used to extract lower dimensional features that have been used for the visualization and de-noising of the signals, although interpreting these features of statistical interest in terms of their biological function or correlates remains a challenge.

Recently, graph theoretic approaches have enabled considerable advances to be made in understanding the organization of functional and anatomical connections in the brain (Van Wijk et al., 2010). Using these approaches, the graph of functional correlates of LFP signals can be evaluated to find clusters of connectivity, central hubs, and other graph features, and to study how network properties vary with different conditions. The advent of parallel LFP recordings necessitates the development of advanced computational tools that can deal with high-dimensional data, to yield future novel insights into the inner workings of the brain.

Summary

With nearly 100 billion neurons and 100 trillion connections, how the brains circuits enable its function remains one of the greatest unsolved enigmas in science and engineering. In recent years, electrical neural interfaces have been developed to support the interrogation of highly complex brain circuits that can involve vast numbers of neurons at diverse spatiotemporal scales. In this review, we discuss exciting recent advances in multiple areas of electrical neural interface development, including the design of neural electrodes that record at larger spatial scales and over longer durations, novel mechanisms that permit wireless interfaces, specialized ASICs that allow more efficient interfaces, the integration of electrical interfaces with optical methods to improve resolution and coverage, and the creation of algorithms to extract features from neural recordings. The application of these advances has markedly improved our capability to interact with the nervous system.

We envision that electrical neural interfaces will continue to be of paramount importance for neuroengineering and neuroscience, and need breakthrough innovations to address key technical challenges. Further improvements in their spatiotemporal scales is of top importance. For instance, extending stable recording period of individual neurons from months to lifetime could enable a number of exciting clinical applications; a massive scaling of the number of neurons being simultaneously recorded in a brain could lead to a paradigm shift in neuroscience studies (Kleinfeld et al., 2019). Further, we will also need to engineer integrated electronics that are compact and power efficient, and to develop innovative approaches for wireless transmission. Meanwhile, the ever-growing dimensions and diversity of neural data necessitate a drastic improvement in algorithms. While many of

these challenges appear daunting, we do not foresee any limitations imposed by fundamental underlying physical principles. Lastly, we emphasize that the timely dissemination of new technology, which requires joint effort and close collaboration between academia and industry, is equally important.

Acknowledgments

Funding: This work was supported by the National Institute of Neurological Disorders and Stroke grants R01NS102917 (C.X.), U01NS115588 (C.X.), R01NS109361 (L.L.), and U01NS108680 (B.A.), by the National Institute Of Biomedical Imaging And Bioengineering grant U18EB029353 (J.T.R and K.Y.), by the National Science Foundation grant ECCS-2023849 (J.T.R. and K.Y.), and by the Welch foundation Research grant #F-1941-20170325 (C.X.).

Uncategorized References

A. Gilletti JM (2006). Brain micromoation around implants in the rodent somatosensory cortex. Journal of Neural Engineering 3, 189–195. [PubMed: 16921202]

Abdelfattah AS, Kawashima T, Singh A, Novak O, Liu H, Shuai Y, Huang YC, Campagnola L, Seeman SC, Yu J, et al. (2019). Bright and photostable chemigenetic indicators for extended in vivo voltage imaging. Science 365, 699–704. [PubMed: 31371562]

Adam Y, Kim JJ, Lou S, Zhao Y, Xie ME, Brinks D, Wu H, Mostajo-Radji MA, Kheifets S, Parot V, et al. (2019). Voltage imaging and optogenetics reveal behaviour-dependent changes in hippocampal dynamics. Nature 569, 413–417. [PubMed: 31043747]

Agrawal DR, Tanabe Y, Weng D, Ma A, Hsu S, Liao SY, Zhen Z, Zhu ZY, Sun C, Dong Z, et al. (2017). Conformal phased surfaces for wireless powering of bioelectronic microdevices. Nature Biomedical Engineering 1, 1–16.

Alivisatos AP, Chun M, Church GM, Greenspan RJ, Roukes ML, and Yuste R (2012). The brain activity map project and the challenge of functional connectomics. Neuron 74, 970–974. [PubMed: 22726828]

Amblard P-O, and Michel OJ (2013). The relation between Granger causality and directed information theory: A review. Entropy 15, 113–143.

Andersen RA, Musallam S, and Pesaran B (2004). Selecting the signals for a brain–machine interface. Current opinion in neurobiology 14, 720–726. [PubMed: 15582374]

Barnett L, and Seth AK (2014). The MVGC multivariate Granger causality toolbox: a new approach to Granger-causal inference. Journal of neuroscience methods 223, 50–68. [PubMed: 24200508]

Barrese JC, Rao N, Paroo K, Triebwasser C, Vargas-Irwin C, Franquemont L, and Donoghue JP (2013a). Failure mode analysis of silicon-based intracortical microelectrode arrays in non-human primates. Journal of Neural Engineering 10.

Barrese JC, Rao N, Paroo K, Triebwasser C, Vargas-Irwin C, Franquemont L, and Donoghue JP (2013b). Failure mode analysis of silicon-based intracortical microelectrode arrays in non-human primates. Journal of neural engineering 10, 066014. [PubMed: 24216311]

Belitski A, Gretton A, Magri C, Murayama Y, Montemurro MA, Logothetis NK, and Panzeri S (2008). Low-frequency local field potentials and spikes in primary visual cortex convey independent visual information. J Neurosci 28, 5696–5709. [PubMed: 18509031]

Benfenati V, Toffanin S, Bonetti S, Turatti G, Pistone A, Chiappalone M, Sagnella A, Stefani A, Generali G, Ruani G, et al. (2013). A transparent organic transistor structure for bidirectional stimulation and recording of primary neurons. Nat Mater 12, 672–680. [PubMed: 23644524]

Biederman W, Yeager DJ, Narevsky N, Leverett J, Neely R, Carmena JM, Alon E, and Rabaey JM (2015). A 4.78 mm 2 Fully-Integrated Neuromodulation SoC Combining 64 Acquisition Channels With Digital Compression and Simultaneous Dual Stimulation. IEEE Journal of Solid-State Circuits 50, 1038–1047.

Birmingham K, Gradinaru V, Anikeeva P, Grill WM, Pikov V, McLaughlin B, Pasricha P, Weber D, Ludwig K, and Famm K (2014). Bioelectronic medicines: a research roadmap. Nature reviews Drug discovery 13, 399–400. [PubMed: 24875080]

Boyden ES, Zhang F, Bamberg E, Nagel G, and Deisseroth K (2005). Millisecond-timescale, genetically targeted optical control of neural activity. Nat Neurosci 8, 1263–1268. [PubMed: 16116447]

Brown EN, Kass RE, and Mitra PP (2004). Multiple neural spike train data analysis: state-of-the-art and future challenges. Nature neuroscience 7, 456–461. [PubMed: 15114358]

Brunton BW, Johnson LA, Ojemann JG, and Kutz JN (2016). Extracting spatial–temporal coherent patterns in large-scale neural recordings using dynamic mode decomposition. Journal of neuroscience methods 258, 1–15. [PubMed: 26529367]

Buzsáki G, Anastassiou CA, and Koch C (2012). The origin of extracellular fields and currents—EEG, ECoG, LFP and spikes. Nature reviews neuroscience 13, 407–420. [PubMed: 22595786]

Cai Z, Neveu CL, Baxter DA, Byrne JH, and Aazhang B (2017). Inferring neuronal network functional connectivity with directed information. Journal of neurophysiology 118, 1055–1069. [PubMed: 28468991]

Canales A, Jia X, Froriep UP, Koppes RA, Tringides CM, Selvidge J, Lu C, Hou C, Wei L, Fink Y, et al. (2015). Multifunctional fibers for simultaneous optical, electrical and chemical interrogation of neural circuits in vivo. Nat Biotechnol 33, 277–284. [PubMed: 25599177]

Chen R, Canales A, and Anikeeva P (2017). Neural Recording and Modulation Technologies. Nat Rev Mater 2.

Chen R, Romero G, Christiansen MG, Mohr A, and Anikeeva P (2015). Wireless magnetothermal deep brain stimulation. Science 347, 1477–1480. [PubMed: 25765068]

Chen TW, Wardill TJ, Sun Y, Pulver SR, Renninger SL, Baohan A, Schreiter ER, Kerr RA, Orger MB, Jayaraman V, et al. (2013). Ultrasensitive fluorescent proteins for imaging neuronal activity. Nature 499, 295–300. [PubMed: 23868258]

Chung JE, Joo HR, Fan JL, Liu DF, Barnett AH, Chen S, Geaghan-Breiner C, Karlsson MP, Karlsson M, Lee KY, et al. (2019). High-Density, Long-Lasting, and Multi-region Electrophysiological Recordings Using Polymer Electrode Arrays. Neuron 101, 21–31 e25 [PubMed: 30502044]

Chung JE, Magland JF, Barnett AH, Tolosa VM, Tooker AC, Lee KY, Shah KG, Felix SH, Frank LM, and Greengard LF (2017). A Fully Automated Approach to Spike Sorting. Neuron 95, 1381–1394 e1386. [PubMed: 28910621]

Collinger JL, Foldes S, Bruns TM, Wodlinger B, Gaunt R, and Weber DJ (2013). Neuroprosthetic technology for individuals with spinal cord injury. The journal of spinal cord medicine 36, 258–272. [PubMed: 23820142]

Cortese AJ, Smart CL, Wang T, Reynolds MF, Norris SL, Ji Y, Lee S, Mok A, Wu C, Xia F, et al. (2020). Microscopic sensors using optical wireless integrated circuits. Proceedings of the National Academy of Sciences 117, 9173–9179.

Csicsvari J, Henze DA, Jamieson B, Harris KD, Sirota A, Bartho P, Wise KD, and Buzsaki G (2003). Massively parallel recording of unit and local field potentials with silicon-based electrodes. Journal of neurophysiology 90, 1314–1323. [PubMed: 12904510]

Cunningham JP, and Byron MY (2014). Dimensionality reduction for large-scale neural recordings. Nature neuroscience 17, 1500. [PubMed: 25151264]

Deng X, Liu DF, Kay K, Frank LM, and Eden UT (2015). Clusterless Decoding of Position from Multiunit Activity Using a Marked Point Process Filter. Neural Comput 27, 1438–1460. [PubMed: 25973549]

Dickey AS, Suminski A, Amit Y, and Hatsopoulos NG (2009). Single-unit stability using chronically implanted multielectrode arrays. Journal of neurophysiology 102, 1331–1339. [PubMed: 19535480]

Dotson NM, Goodell B, Salazar RF, Hoffman SJ, and Gray CM (2015). Methods, caveats and the future of large-scale microelectrode recordings in the non-human primate. Front Syst Neurosci 9, 149. [PubMed: 26578906]

Dragas J, Viswam V, Shadmani A, Chen Y, Bounik R, Stettler A, Radivojevic M, Geissler S, Obien M, Muller J, et al. (2017). A Multi-Functional Microelectrode Array Featuring 59760 Electrodes, 2048 Electrophysiology Channels, Stimulation, Impedance Measurement and Neurotransmitter Detection Channels. IEEE J Solid-State Circuits 52, 1576–1590. [PubMed: 28579632]

Du J, Blanche TJ, Harrison RR, Lester HA, and Masmanidis SC (2011). Multiplexed, High Density Electrophysiology with Nanofabricated Neural Probes. PLOS ONE 6, e26204. [PubMed: 22022568]

Du ZJ, Kolarcik CL, Kozai TD, Luebben SD, Sapp SA, Zheng XS, Nabity JA, and Cui XT (2017). Ultrasoft microwire neural electrodes improve chronic tissue integration. Acta Biomaterialia 53, 46–58. [PubMed: 28185910]

Einevoll GT, Franke F, Hagen E, Pouzat C, and Harris KD (2012). Towards reliable spike-train recordings from thousands of neurons with multielectrodes. Curr Opin Neurobiol 22, 11–17. [PubMed: 22023727]

Einevoll GT, Kayser C, Logothetis NK, and Panzeri S (2013). Modelling and analysis of local field potentials for studying the function of cortical circuits. Nature Reviews Neuroscience 14, 770–785. [PubMed: 24135696]

Eles JR, Vazquez AL, Kozai TDY, and Cui XT (2018). In vivo imaging of neuronal calcium during electrode implantation: Spatial and temporal mapping of damage and recovery. Biomaterials 174, 79–94. [PubMed: 29783119]

Fan B, Rusinek CA, Thompson CH, Setien M, Guo Y, Rechenberg R, Gong Y, Weber AJ, Becker MF, Purcell E, et al. (2020). Flexible, diamond-based microelectrodes fabricated using the diamond growth side for neural sensing. Microsyst Nanoeng 6, 42. [PubMed: 32685185]

Fraser GW, and Schwartz AB (2012). Recording from the same neurons chronically in motor cortex. Journal of neurophysiology 107, 1970–1978. [PubMed: 22190623]

Freeman DK, O'Brien JM, Kumar P, Daniels B, Irion RA, Shraytah L, Ingersoll BK, Magyar AP, Czarnecki A, Wheeler J, et al. (2017). A Sub-millimeter, Inductively Powered Neural Stimulator. Front Neurosci 11, 659. [PubMed: 29230164]

Fu T-M, Hong G, Zhou T, Schuhmann TG, Viveros RD, and Lieber CM (2016). Stable long-term chronic brain mapping at the single-neuron level. Nat Meth 13, 875–882.

Gabrié M, Manoel A, Luneau C, Macris N, Krzakala F, and Zdeborová L (2018). Entropy and mutual information in models of deep neural networks. Paper presented at: Advances in Neural Information Processing Systems.

Gao S, Ver Steeg G, and Galstyan A (2015). Efficient estimation of mutual information for strongly dependent variables. Paper presented at: Artificial intelligence and statistics.

Ghanbari MM, Piech DK, Shen K, Alamouti SF, Yalcin C, Johnson BC, Carmena JM, Maharbiz MM, and Muller R (2019). A Sub-mm3 Ultrasonic Free-Floating Implant for Multi-Mote Neural Recording. IEEE Journal of Solid-State Circuits 54, 3017–3030.

Gilgunn PJ, Ong XC, Flesher SN, Schwartz AB, and Gaunt RA (2013). Structural Analysis of Explanted Microelectrode Arrays. I Ieee Embs C Neur E, 719–722.

Gilletti A, and Muthuswamy J (2006). Brain micromotion around implants in the rodent somatosensory cortex. J Neural Eng 3, 189–195. [PubMed: 16921202]

Gold C, Henze DA, Koch C, and Buzsaki G (2006). On the origin of the extracellular action potential waveform: A modeling study. Journal of neurophysiology 95, 3113–3128. [PubMed: 16467426]

Guan S, Wang J, Gu X, Zhao Y, Hou R, Fan H, Zou L, Gao L, Du M, Li C, et al. (2019). Elastocapillary self-assembled neurotassels for stable neural activity recordings. Science Advances 5, eaav2842. [PubMed: 30944856]

Guitchounts G, Markowitz JE, Liberti WA, and Gardner TJ (2013). A carbon-fiber electrode array for long-term neural recording. Journal of neural engineering 10, 046016. [PubMed: 23860226]

Guo ZV, Li N, Huber D, Ophir E, Gutnisky D, Ting JT, Feng G, and Svoboda K (2014). Flow of cortical activity underlying a tactile decision in mice. Neuron 81, 179–194. [PubMed: 24361077]

Ha S, Akinin A, Park J, Kim C, Wang H, Maier C, Mercier PP, and Cauwenberghs G (2017). Silicon-Integrated High-Density Electrocortical Interfaces. Proceedings of the IEEE 105, 11–33.

Hanson TL, Diaz-Botia CA, Kharazia V, Maharbiz MM, and Sabes PN (2019). The "sewing machine" for minimally invasive neural recording. bioRxiv.

Hargreaves DG, Drew SJ, and Eckersley R (2004). Kirschner Wire Pin Tract Infection Rates: A randomized controlled trial between percutaneous and buried wires. The Journal of Hand Surgery: British & European Volume 29, 374–376.

He F, Sullender CT, Zhu H, Williamson MR, Li X, Zhao Z, Jones TA, Xie C, Dunn AK, and Luan L (2020). Multimodal mapping of neural activity and cerebral blood flow reveals long-lasting neurovascular dissociations after small-scale strokes. Sci Adv In press

Helmchen F, and Denk W (2005). Deep tissue two-photon microscopy. Nat Methods 2, 932–940. [PubMed: 16299478]

Henze DA, Borhegyi Z, Csicsvari J, Mamiya A, Harris KD, and Buzsaki G (2000). Intracellular features predicted by extracellular recordings in the hippocampus in vivo. Journal of neurophysiology 84, 390–400. [PubMed: 10899213]

Hong G, Fu T-M, Qiao M, Viveros RD, Yang X, Zhou T, Lee JM, Park H-G, Sanes JR, and Lieber CM (2018). A method for single-neuron chronic recording from the retina in awake mice. Science 360, 1447–1451. [PubMed: 29954976]

Jerison HJ (1992). Anatomy of the Cortex - Statistics and Geometry - Braitenberg V, Schuz A. Contemp Psychol 37, 927–928.

Jia Y, Mirbozorgi SA, Lee B, Khan W, Madi F, Inan OT, Weber A, Li W, and Ghovanloo M (2019). A mm-Sized Free-Floating Wirelessly Powered Implantable Optical Stimulation Device. IEEE Trans Biomed Circuits Syst 13, 608–618. [PubMed: 31135371]

Joo HR, Fan JL, Chen S, Pebbles JA, Liang H, Chung JE, Yorita AM, Tooker AC, Tolosa VM, Geaghan-Breiner C, et al. (2019). A microfabricated, 3D-sharpened silicon shuttle for insertion of flexible electrode arrays through dura mater into brain. J Neural Eng 16, 066021. [PubMed: 31216526]

Jorfi M, Skousen JL, Weder C, and Capadona JR (2015). Progress towards biocompatible intracortical microelectrodes for neural interfacing applications. J Neural Eng 12, 011001. [PubMed: 25460808]

Jun JJ, Steinmetz NA, Siegle JH, Denman DJ, Bauza M, Barbarits B, Lee AK, Anastassiou CA, Andrei A, Aydin Ç, et al. (2017). Fully integrated silicon probes for high-density recording of neural activity. Nature 551, 232. [PubMed: 29120427]

Kajikawa Y, and Schroeder CE (2011). How local is the local field potential? Neuron 72, 847–858. [PubMed: 22153379]

Karumbaiah L, Saxena T, Carlson D, Patil K, Patkar R, Gaupp EA, Betancur M, Stanley GB, Carin L, and Bellamkonda RV (2013). Relationship between intracortical electrode design and chronic recording function. Biomaterials 34, 8061–8074. [PubMed: 23891081]

Khalifa A, Liu Y, Karimi Y, Wang Q, Eisape A, Stanacevic M, Thakor N, Bao Z, and Etienne-Cummings R (2019). The Microbead: A 0.009 mm(3) Implantable Wireless Neural Stimulator. IEEE Trans Biomed Circuits Syst 13, 971–985. [PubMed: 31484132]

Khodagholy D, Gelinas JN, Thesen T, Doyle W, Devinsky O, Malliaras GG, and Buzsaki G (2015). NeuroGrid: recording action potentials from the surface of the brain. Nat Neurosci 18, 310–315. [PubMed: 25531570]

Kilias A, Canales A, Froriep UP, Park S, Egert U, and Anikeeva P (2018). Optogenetic entrainment of neural oscillations with hybrid fiber probes. J Neural Eng 15, 056006. [PubMed: 29923505]

Kipke DR, Vetter RJ, Williams JC, and Hetke JF (2003). Silicon-substrate intracortical microelectrode arrays for long-term recording of neuronal spike activity in cerebral cortex. IEEE transactions on neural systems and rehabilitation engineering : a publication of the IEEE Engineering in Medicine and Biology Society 11, 151–155.

Kleinfeld D, Luan L, Mitra PP, Robinson JT, Sarpeshkar R, Shepard K, Xie C, and Harris TD (2019). Can One Concurrently Record Electrical Spikes from Every Neuron in a Mammalian Brain? Neuron 103, 1005–1015. [PubMed: 31495645]

Kozai TD, Catt K, Li X, Gugel ZV, Olafsson VT, Vazquez AL, and Cui XT (2015a). Mechanical failure modes of chronically implanted planar silicon-based neural probes for laminar recording. Biomaterials 37, 25–39. [PubMed: 25453935]

Kozai TD, Jaquins-Gerstl AS, Vazquez AL, Michael AC, and Cui XT (2015b). Brain tissue responses to neural implants impact signal sensitivity and intervention strategies. ACS chemical neuroscience 6, 48–67. [PubMed: 25546652]

Kozai TD, and Vazquez AL (2015). Photoelectric artefact from optogenetics and imaging on microelectrodes and bioelectronics: New Challenges and Opportunities. J Mater Chem B 3, 4965–4978. [PubMed: 26167283]

Kozai TDY, Langhals NB, Patel PR, Deng X, Zhang H, Smith KL, Lahann J, Kotov NA, and Kipke DR (2012). Ultrasmall implantable composite microelectrodes with bioactive surfaces for chronic neural interfaces. Nature materials 11, 1065–1073. [PubMed: 23142839]

Kreiman G, Hung CP, Kraskov A, Quiroga RQ, Poggio T, and DiCarlo JJ (2006). Object selectivity of local field potentials and spikes in the macaque inferior temporal cortex. Neuron 49, 433–445. [PubMed: 16446146]

Kuzum D, Takano H, Shim E, Reed JC, Juul H, Richardson AG, de Vries J, Bink H, Dichter MA, Lucas TH, et al. (2014). Transparent and flexible low noise graphene electrodes for simultaneous electrophysiology and neuroimaging. Nat Commun 5, 5259. [PubMed: 25327632]

Lee J, Ozden I, Song YK, and Nurmikko AV (2015). Transparent intracortical microprobe array for simultaneous spatiotemporal optical stimulation and multichannel electrical recording. Nat Methods 12, 1157–1162. [PubMed: 26457862]

Lee S, Cortese AJ, Gandhi AP, Agger ER, McEuen PL, and Molnar AC (2018a). A 250 μm × 57 μm Microscale Opto-electronically Transduced Electrodes (MOTEs) for Neural Recording. IEEE Transactions on Biomedical Circuits and Systems 12, 1256–1266. [PubMed: 30334768]

Lee S, Cortese AJ, Trexel P, Agger ER, McEuen PL, and Molnar AC (2018b). A 330μm×90μm Opto-Electronically Integrated Wireless System-on-Chip for Recording of Neural Activities Sunwoo. 2018 IEEE International Solid-State Circuits Conference, 292–294.

Lee W, Croce P, Margolin RW, Cammalleri A, Yoon K, and Yoo SS (2018c). Transcranial focused ultrasound stimulation of motor cortical areas in freely-moving awake rats. BMC Neuroscience 19, 1–14. [PubMed: 29338692]

Lee W, Kim D, Matsuhisa N, Nagase M, Sekino M, Malliaras GG, Yokota T, and Someya T (2017). Transparent, conformable, active multielectrode array using organic electrochemical transistors. Proc Natl Acad Sci U S A 114, 10554–10559. [PubMed: 28923928]

Lemon R (1984). Methods for Neuronal Recording in Conscious Animals (Chichester: John Wiley and Sons).

Lewicki MS (1998). A review of methods for spike sorting: the detection and classification of neural action potentials. Network 9, R53–78. [PubMed: 10221571]

Lim J, Moon E, Barrow M, Nason SR, Patel PR, Patil PG, Oh S, Lee I, Kim H, Sylvester D, et al. (2020). 26.9 A 0.19×0.17mm2 Wireless Neural Recording IC for Motor Prediction with Near-Infrared-Based Power and Data Telemetry. Paper presented at: 2020 IEEE International Solid-State Circuits Conference - (ISSCC).

Lin MZ, and Schnitzer MJ (2016). Genetically encoded indicators of neuronal activity. Nat Neurosci 19, 1142–1153. [PubMed: 27571193]

Lindén H, Tetzlaff T, Potjans TC, Pettersen KH, Grün S, Diesmann M, and Einevoll GT (2011). Modeling the spatial reach of the LFP. Neuron 72, 859–872. [PubMed: 22153380]

Liu J, Fu TM, Cheng Z, Hong G, Zhou T, Jin L, Duvvuri M, Jiang Z, Kruskal P, Xie C, et al. (2015). Syringe-injectable electronics. Nature nanotechnology 10, 629–636.

Liu J, Xie C, Dai X, Jin L, Zhou W, and Lieber CM (2013). Multifunctional three-dimensional macroporous nanoelectronic networks for smart materials. Proc Natl Acad Sci USA 110, 6694–6699. [PubMed: 23569270]

Liu X, Zhang M, Richardson AG, Lucas TH, and Spiegel J.V.d. (2017). Design of a Closed-Loop, Bidirectional Brain Machine Interface System With Energy Efficient Neural Feature Extraction and PID Control. IEEE Transactions on Biomedical Circuits and Systems 11, 729–742. [PubMed: 28029630]

Lopez CM, Putzeys J, Raducanu BC, Ballini M, Wang S, Andrei A, Rochus V, Vandebriel R, Severi S, Hoof CV, et al. (2017). A Neural Probe With Up to 966 Electrodes and Up to 384 Configurable Channels in 0.13 μm SOI CMOS. IEEE Transactions on Biomedical Circuits and Systems 11, 510–522. [PubMed: 28422663]

Luan L, Sullender CT, Li X, Zhao Z, Zhu H, Wei X, Xie C, and Dunn AK (2018). Nanoelectronics enabled chronic multimodal neural platform in a mouse ischemic model. Journal of neuroscience methods 295, 68–76. [PubMed: 29203409]

Luan L, Wei X, Zhao Z, Siegel JJ, Potnis O, Tuppen CA, Lin S, Kazmi S, Fowler RA, Holloway S, et al. (2017). Ultraflexible nanoelectronic probes form reliable, glial scar-free neural integration. Sci Adv 3, e1601966. [PubMed: 28246640]

Ludwig KA, Miriani RM, Langhals NB, Joseph MD, Anderson DJ, and Kipke DR (2009). Using a common average reference to improve cortical neuron recordings from microelectrode arrays. Journal of neurophysiology 101, 1679–1689. [PubMed: 19109453]

Malladi R, Kalamangalam G, Tandon N, and Aazhang B (2016). Identifying seizure onset zone from the causal connectivity inferred using directed information. IEEE Journal of Selected Topics in Signal Processing 10, 1267–1283.

Massey TL, Santacruz SR, Hou JF, Pister KSJ, Carmena JM, and Maharbiz MM (2019). A high-density carbon fiber neural recording array technology. Journal of Neural Engineering 16, 016024. [PubMed: 30524060]

Melosh N (2019). presentation at Brain Investigator Annual meeting.

Mercanzini A, Cheung K, Buhl DL, Boers M, Maillard A, Colin P, Bensadoun J-C, Bertsch A, and Renaud P (2008). Demonstration of cortical recording using novel flexible polymer neural probes. Sensors and Actuators A: Physical 143, 90–96.

Montgomery KL, Yeh AJ, Ho JS, Tsao V, Mohan Iyer S, Grosenick L, Ferenczi EA, Tanabe Y, Deisseroth K, Delp SL, et al. (2015). Wirelessly powered, fully internal optogenetics for brain, spinal and peripheral circuits in mice. Nat Meth 12, 969–974.

Mora Lopez C, Putzeys J, Raducanu BC, Ballini M, Wang S, Andrei A, Rochus V, Vandebriel R, Severi S, Van Hoof C, et al. (2017). A Neural Probe With Up to 966 Electrodes and Up to 384 Configurable Channels in 0.13 μm SOI CMOS. IEEE Trans Biomed Circuits Syst 11, 510–522. [PubMed: 28422663]

Mukamel R, Gelbard H, Arieli A, Hasson U, Fried I, and Malach R (2005). Coupling between neuronal firing, field potentials, and FMRI in human auditory cortex. Science 309, 951–954. [PubMed: 16081741]

Musk E, and Neuralink (2019). An Integrated Brain-Machine Interface Platform With Thousands of Channels. J Med Internet Res 21, e16194. [PubMed: 31642810]

Nan T, Lin H, Gao Y, Matyushov A, Yu G, Chen H, Sun N, Wei S, Wang Z, Li M, et al. (2017). Acoustically actuated ultra-compact NEMS magnetoelectric antennas. Nature Communications 8, 1–7.

Nicolelis MA (2001). Actions from thoughts. Nature 409, 403–407. [PubMed: 11201755]

Nicolelis MA, Dimitrov D, Carmena JM, Crist R, Lehew G, Kralik JD, and Wise SP (2003). Chronic, multisite, multielectrode recordings in macaque monkeys. Proc Natl Acad Sci U S A 100, 11041–11046. [PubMed: 12960378]

Obaid A, Hanna M-E, Wu Y-W, Kollo M, Racz R, Angle MR, Möller J, Brackbill N, Wray W, Franke F, et al. (2020). Massively parallel microwire arrays integrated with CMOS chips for neural recording. Science Advances 6, eaay2789. [PubMed: 32219158]

P. Rousche RN (1992). A method for pneumatically inserting an array of penetrating electrodes into cortical tissue. Annals of Biomedical Engineering 20, 413–422. [PubMed: 1510293]

Pachitariu M, Steinmetz N, Kadir S, Carandini M, and Kenneth D,H (2016). Kilosort: realtime spike-sorting for extracellular electrophysiology with hundreds of channels. bioRxiv, 061481.

Pachitariu M, Steinmetz N, Kadir SN, Carandini M, and Kenneth D,H (2019). Kilosort2: automated spike sorting with drift tracking and template matching on GPUs. https://githubcom/MouseLand/Kilosort2.

Park DW, Brodnick SK, Ness JP, Atry F, Krugner-Higby L, Sandberg A, Mikael S, Richner TJ, Novello J, Kim H, et al. (2016a). Fabrication and utility of a transparent graphene neural electrode array for electrophysiology, in vivo imaging, and optogenetics. Nat Protoc 11, 2201–2222. [PubMed: 27735935]

Park J, Jin K, Sahasrabudhe A, Chiang PH, Maalouf JH, Koehler F, Rosenfeld D, Rao S, Tanaka T, Khudiyev T, et al. (2020a). In situ electrochemical generation of nitric oxide for neuronal modulation. Nature nanotechnology 15, 690–697.

Park JH, Tan JSY, Wu H, and Yoo J (2020b). 34.2 1225-Channel Localized Temperature-Regulated Neuromorphic Retinal-Prosthesis SoC with 56.3nW/Channel Image Processor. Paper presented at: 2020 IEEE International Solid- State Circuits Conference - (ISSCC).

Park S, Guo Y, Jia X, Choe HK, Grena B, Kang J, Park J, Lu C, Canales A, Chen R, et al. (2017). One-step optogenetics with multifunctional flexible polymer fibers. Nat Neurosci 20, 612–619. [PubMed: 28218915]

Park S-Y, Cho J, Na K, and Yoon E (2018). Modular 128-Channel Δ - $\Delta \Sigma$ Analog Front-End Architecture Using Spectrum Equalization Scheme for 1024-Channel 3-D Neural Recording Microsystems. IEEE Journal of Solid-State Circuits 53, 501–514.

Park SI, Shin G, McCall JG, Al-Hasani R, Norris A, Xia L, Brenner DS, Noh KN, Bang SY, Bhatti DL, et al. (2016b). Stretchable multichannel antennas in soft wireless optoelectronic implants for optogenetics. Proc Natl Acad Sci U S A 113, E8169–E8177. [PubMed: 27911798]

Patel PR, Na K, Zhang H, Kozai TD, Kotov NA, Yoon E, and Chestek CA (2015). Insertion of linear 8.4 mum diameter 16 channel carbon fiber electrode arrays for single unit recordings. J Neural Eng 12, 046009. [PubMed: 26035638]

Perge JA, Homer ML, Malik WQ, Cash S, Eskandar E, Friehs G, Donoghue JP, and Hochberg LR (2013). Intra-day signal instabilities affect decoding performance in an intracortical neural interface system. J Neural Eng 10, 036004. [PubMed: 23574741]

Perlmutter JS, and Mink JW (2006). Deep brain stimulation. Annual review of neuroscience 29, 229–257.

Pesaran B, Pezaris JS, Sahani M, Mitra PP, and Andersen RA (2002). Temporal structure in neuronal activity during working memory in macaque parietal cortex. Nat Neurosci 5, 805–811. [PubMed: 12134152]

Pesaran B, Vinck M, Einevoll GT, Sirota A, Fries P, Siegel M, Truccolo W, Schroeder CE, and Srinivasan R (2018). Investigating large-scale brain dynamics using field potential recordings: analysis and interpretation. Nature neuroscience 21, 903–919. [PubMed: 29942039]

Peterka DS, Takahashi H, and Yuste R (2011). Imaging voltage in neurons. Neuron 69, 9–21. [PubMed: 21220095]

Piech DK, Johnson BC, Shen K, Ghanbari MM, Li KY, Neely RM, Kay JE, Carmena JM, and Maharbiz MM (2020). A wireless millimetre-scale implantable neural stimulator with ultrasonically powered bidirectional communication. Nature Biomedical Engineering 4, 207–222.

Poskanzer KE, and Yuste R (2016). Astrocytes regulate cortical state switching in vivo. Proc Natl Acad Sci U S A 113, E2675–2684. [PubMed: 27122314]

Potworowski J, Jakuczun W, Łęski S, and Wójcik D (2012). Kernel current source density method. Neural computation 24, 541–575. [PubMed: 22091662]

Prasad A, Xue QS, Dieme R, Sankar V, Mayrand RC, Nishida T, Streit WJ, and Sanchez JC (2014). Abiotic-biotic characterization of Pt/Ir microelectrode arrays in chronic implants. Frontiers in neuroengineering 7, 2. [PubMed: 24550823]

Prasad A, Xue QS, Sankar V, Nishida T, Shaw G, Streit WJ, and Sanchez JC (2012). Comprehensive characterization and failure modes of tungsten microwire arrays in chronic neural implants. J Neural Eng 9, 056015. [PubMed: 23010756]

Rahmani H, and Babakhani A (2017). A wireless power receiver with an on-chip antenna for millimeter-size biomedical implants in 180 nm SOI CMOS. IEEE MTT-S International Microwave Symposium Digest, 300–303.

Reddy JW, Kimukin I, Stewart LT, Ahmed Z, Barth AL, Towe E, and Chamanzar M (2019). High Density, Double-Sided, Flexible Optoelectronic Neural Probes With Embedded muLEDs. Front Neurosci 13, 745. [PubMed: 31456654]

Rios G, Lubenov EV, Chi D, Roukes ML, and Siapas AG (2016). Nanofabricated Neural Probes for Dense 3-D Recordings of Brain Activity. Nano Lett 16, 6857–6862. [PubMed: 27766885]

Rossant C, Kadir SN, Goodman DFM, Schulman J, Hunter MLD, Saleem AB, Grosmark A, Belluscio M, Denfield GH, Ecker AS, et al. (2016). Spike sorting for large, dense electrode arrays. Nat Neurosci 19, 634–641. [PubMed: 26974951]

Rousche PJ, and Normann RA (1998). Chronic recording capability of the Utah Intracortical Electrode Array in cat sensory cortex. Journal of neuroscience methods 82, 1–15. [PubMed: 10223510]

Scherberger H, Jarvis MR, and Andersen RA (2005). Cortical local field potential encodes movement intentions in the posterior parietal cortex. Neuron 46, 347–354. [PubMed: 15848811]

Scholvin J, Kinney JP, Bernstein JG, Moore-Kochlacs C, Kopell N, Fonstad CG, and Boyden ES (2016). Close-Packed Silicon Microelectrodes for Scalable Spatially Oversampled Neural Recording. IEEE Transactions on Biomedical Engineering 63, 120–130. [PubMed: 26699649]

Schouenborg J, Garwicz M, and Danielsen N (2011). Reducing surface area while maintaining implant penetrating profile lowers the brain foreign body response to chronically implanted planar silicon microelectrode arrays. Brain Machine Interfaces: Implications for Science, Clinical Practice and Society 194, 167.

Seo D, Carmena JM, Rabaey JM, Maharbiz MM, and Alon E (2015). Model validation of untethered, ultrasonic neural dust motes for cortical recording. Journal of neuroscience methods 244, 114–122. [PubMed: 25109901]

Seo D, Neely RM, Shen K, Rabaey JM, Carmena JM, Maharbiz MM, Seo D, Neely RM, Shen K, Singhal U, et al. (2016). Wireless Recording in the Peripheral Nervous System with Ultrasonic Neural Dust. Neuron 91, 529–539. [PubMed: 27497221]

Seymour EC, Freedman DS, Gokkavas M, Ozbay E, Sahin M, and Unlu MS (2014). Improved selectivity from a wavelength addressable device for wireless stimulation of neural tissue. Frontiers in neuroengineering 7, 5. [PubMed: 24600390]

Seymour JP, and Kipke DR (2007). Neural probe design for reduced tissue encapsulation in CNS. Biomaterials 28, 3594–3607. [PubMed: 17517431]

Shen H (2013). Neurotechnology: BRAIN storm. Nature 503, 26–28. [PubMed: 24201265]

Shew WL, Bellay T, and Plenz D (2010). Simultaneous multi-electrode array recording and two-photon calcium imaging of neural activity. Journal of neuroscience methods 192, 75–82. [PubMed: 20659501]

Shin G, Gomez AM, Al-Hasani R, Jeong YR, Kim J, Xie Z, Banks A, Lee SM, Han SY, Yoo CJ, et al. (2017). Flexible Near-Field Wireless Optoelectronics as Subdermal Implants for Broad Applications in Optogenetics. Neuron 93, 509–521.e503. [PubMed: 28132830]

Shulyzki R, Abdelhalim K, Bagheri A, Salam MT, Florez CM, Velazquez JL, Carlen PL, and Genov R (2015). 320-channel active probe for high-resolution neuromonitoring and responsive neurostimulation. IEEE Trans Biomed Circuits Syst 9, 34–49. [PubMed: 25486647]

Simeral JD, Kim SP, Black MJ, Donoghue JP, and Hochberg LR (2011). Neural control of cursor trajectory and click by a human with tetraplegia 1000 days after implant of an intracortical microelectrode array. Journal of Neural Engineering 8.

Singer A, Dutta S, Lewis E, Chen Z, Chen JC, Verma N, Avants B, Feldman AK, O'Malley J, Beierlein M, et al. (2020). Magnetoelectric Materials for Miniature , Wireless Neural Stimulation at Therapeutic Frequencies. Neuron.

Sohal HS, Clowry GJ, Jackson A, O'Neill A, and Baker SN (2016). Mechanical Flexibility Reduces the Foreign Body Response to Long-Term Implanted Microelectrodes in Rabbit Cortex. PLOS ONE 11, e0165606. [PubMed: 27788240]

Spira ME, and Hai A (2013). Multi-electrode array technologies for neuroscience and cardiology. Nature nanotechnology 8, 83–94.

Stevenson IH, and Kording KP (2011). How advances in neural recording affect data analysis. Nature neuroscience 14, 139. [PubMed: 21270781]

Stosiek C, Garaschuk O, Holthoff K, and Konnerth A (2003). In vivo two-photon calcium imaging of neuronal networks. Proc Natl Acad Sci U S A 100, 7319–7324. [PubMed: 12777621]

Subbaroyan J, Martin DC, and Kipke DR (2005). A finite-element model of the mechanical effects of implantable microelectrodes in the cerebral cortex. J Neural Eng 2, 103–113. [PubMed: 16317234]

Suner S, Fellows MR, Vargas-Irwin C, Nakata GK, and Donoghue JP (2005). Reliability of signals from a chronically implanted, silicon-based electrode array in non-human primate primary motor cortex. IEEE transactions on neural systems and rehabilitation engineering : a publication of the IEEE Engineering in Medicine and Biology Society 13, 524–541.

Szarowski DH, Andersen MD, Retterer S, Spence AJ, Isaacson M, Craighead HG, Turner JN, and Shain W (2003). Brain responses to micro-machined silicon devices. Brain Res 983, 23–35. [PubMed: 12914963]

Taghvayi NE, and Aazhang B (2019). Application of Embedded Dynamic Mode Decomposition on Epileptic Data for Seizure Prediction. Paper presented at: 2019 53rd Asilomar Conference on Signals, Systems, and Computers (IEEE).

Taylor IM, Patel NA, Freedman NC, Castagnola E, and Cui XT (2019). Direct in Vivo Electrochemical Detection of Resting Dopamine Using Poly(3,4-ethylenedioxythiophene)/Carbon Nanotube Functionalized Microelectrodes. Anal Chem 91, 12917–12927. [PubMed: 31512849]

Thunemann M, Lu Y, Liu X, Kilic K, Desjardins M, Vandenberghe M, Sadegh S, Saisan PA, Cheng Q, Weldy KL, et al. (2018). Deep 2-photon imaging and artifact-free optogenetics through transparent graphene microelectrode arrays. Nat Commun 9, 2035. [PubMed: 29789548]

Tian B, Liu J, Dvir T, Jin L, Tsui JH, Qing Q, Suo Z, Langer R, Kohane DS, and Lieber CM (2012). Macroporous nanowire nanoelectronic scaffolds for synthetic tissues. Nat Mater 11, 986–994. [PubMed: 22922448]

Trautmann EM, Stavisky SD, Lahiri S, Ames KC, Kaufman MT, O'Shea DJ, Vyas S, Sun X, Ryu SI, Ganguli S, et al. (2019). Accurate Estimation of Neural Population Dynamics without Spike Sorting. Neuron 103, 292–308 e294. [PubMed: 31171448]

Tsai D, Sawyer D, Bradd A, Yuste R, and Shepard KL (2017). A very large-scale microelectrode array for cellular-resolution electrophysiology. Nature Communications 8, 1802.

Van Wijk BC, Stam CJ, and Daffertshofer A (2010). Comparing brain networks of different size and connectivity density using graph theory. PloS one 5.

Vitale F, Summerson SR, Aazhang B, Kemere C, and Pasquali M (2015). Neural Stimulation and Recording with Bidirectional, Soft Carbon Nanotube Fiber Microelectrodes. ACS Nano 9, 4465–4474. [PubMed: 25803728]

Wei X, Luan L, Zhao Z, Li X, Zhu H, Potnis O, and Xie C (2018). Nanofabricated Ultraflexible Electrode Arrays for High-Density Intracortical Recording. Advanced Science, 1700625. [PubMed: 29938162]

Whitmore NW, and Lin S-C (2016). Unmasking local activity within local field potentials (LFPs) by removing distal electrical signals using independent component analysis. Neuroimage 132, 79–92. [PubMed: 26899209]

Williams JC, Rennaker RL, and Kipke DR (1999). Long-term neural recording characteristics of wire microelectrode arrays implanted in cerebral cortex. Brain research Brain research protocols 4, 303–313. [PubMed: 10592339]

Wise K, and Angell J (1971). A microprobe with integrated amplifiers for neurophysiology. Paper presented at: 1971 IEEE International Solid-State Circuits Conference Digest of Technical Papers.

Wu F, Stark E, Ku PC, Wise KD, Buzsaki G, and Yoon E (2015a). Monolithically Integrated muLEDs on Silicon Neural Probes for High-Resolution Optogenetic Studies in Behaving Animals. Neuron 88, 1136–1148. [PubMed: 26627311]

Wu F, Tien LW, Chen F, Berke JD, Kaplan DL, and Yoon E (2015b). Silk-Backed Structural Optimization of High-Density Flexible Intracortical Neural Probes. Journal of Microelectromechanical Systems 24, 62–69.

Xie C, Liu J, Fu T-M, Dai X, Zhou W, and Lieber CM (2015). Three-dimensional macroporous nanoelectronic networks as minimally invasive brain probes. Nature Materials 14, 1286–1292. [PubMed: 26436341]

Yang X, Zhou T, Zwang TJ, Hong G, Zhao Y, Viveros RD, Fu TM, Gao T, and Lieber CM (2019). Bioinspired neuron-like electronics. Nat Mater 18, 510–517. [PubMed: 30804509]

Yeon P, Bakir MS, and Ghovanloo M (2018). Towards a 1.1 mm2 free-floating wireless implantable neural recording SoC. Paper presented at: 2018 IEEE Custom Integrated Circuits Conference (CICC).

Yger P, Spampinato GL, Esposito E, Lefebvre B, Deny S, Gardella C, Stimberg M, Jetter F, Zeck G, Picaud S, et al. (2018). A spike sorting toolbox for up to thousands of electrodes validated with ground truth recordings in vitro and in vivo. Elife 7.

Yu Z, Chen JC, Avants BW, He Y, Robinson JT, and Yang K (2020a). An 8.2mm 3 Implantable Neurostimulator with Magnetoelectric Power and Data Transfer. Paper presented at: International Solid-State Circuits Conference.

Yu Z, Chen JC, Avants BW, He Y, Singer A, Robinson JT, and Yang K (2020b). 34.3 An 8.2mm3 Implantable Neurostimulator with Magnetoelectric Power and Data Transfer. Paper presented at: 2020 IEEE International Solid- State Circuits Conference - (ISSCC).

Zhang J, Liu X, Xu W, Luo W, Li M, Chu F, Xu L, Cao A, Guan J, Tang S, et al. (2018). Stretchable Transparent Electrode Arrays for Simultaneous Electrical and Optical Interrogation of Neural Circuits in Vivo. Nano Lett 18, 2903–2911. [PubMed: 29608857]

Zhao Z, Li X, He F, Wei X, Lin S, and Xie C (2019). Parallel, minimally-invasive implantation of ultra-flexible neural electrode arrays. Journal of Neural Engineering 16, 035001. [PubMed: 30736013]

Zhao Z, Luan L, Wei X, Zhu H, Li X, Lin S, Siegel JJ, Chitwood RA, and Xie C (2017). Nanoelectronic Coating Enabled Versatile Multifunctional Neural Probes. Nano Lett 17, 4588–4595. [PubMed: 28682082]

Box 1:

Spatial, temporal, and compositional diversity present challenges to electrical neural interface design

Spatial scales.

Neural circuits span wide spatial scales in the brain: they consist of nearby clusters of neurons, as well as neurons distributed across multiple brain areas. On the microscale, we need high spatial resolution in three dimensions (3D) to capture local information processing. This is because each cortical neuron receives 3000 – 10,000 synaptic contacts, more than half of which are thought to arise from neurons within a 100 – 200 μm radius of the target cell (Jerison, 1992). On the macroscale, we need large scale and flexibly distributed coverage to detect neural dynamics at a high density, in not just one region but across multiple regions.

Time scales.

Neural activity occurs across broad time scales in the brain: moment-by-moment information processing takes place on the timescale of milliseconds to seconds, reflecting synaptic transmission and spiking. In addition, changes in activity patterns that support adaptation, learning, memory, development, injury, and degeneration can occur throughout a lifetime and on timescales ranging from seconds (synaptic strength), days to months (circuit remodeling) to years (development and degeneration). Timescales and spatial scales both also vary, sometimes by orders of magnitude, with the subject organism's size and lifespan.

Anatomical diversity.

Brain structure and organization is remarkably different across species and varies across individuals. Functionally distinct brain regions have unique anatomical organization, including tissue geometry, cell types – both neuronal and non-neuronal, cell density, and indeed cellular shape and complexity with various physiological and developmental stages. Furthermore, the brain's neural networks consist of a large number of neurons and also an equal number or more of supportive glial cells, and a dense vascular network that the cells interact with. The challenge in monitoring and especially in manipulating the activity of neural networks with such varying composition is, predominantly, one of attaining spatio-temporal precision in design, during implantation, operation and data processing steps of electrical neural interface engineering.

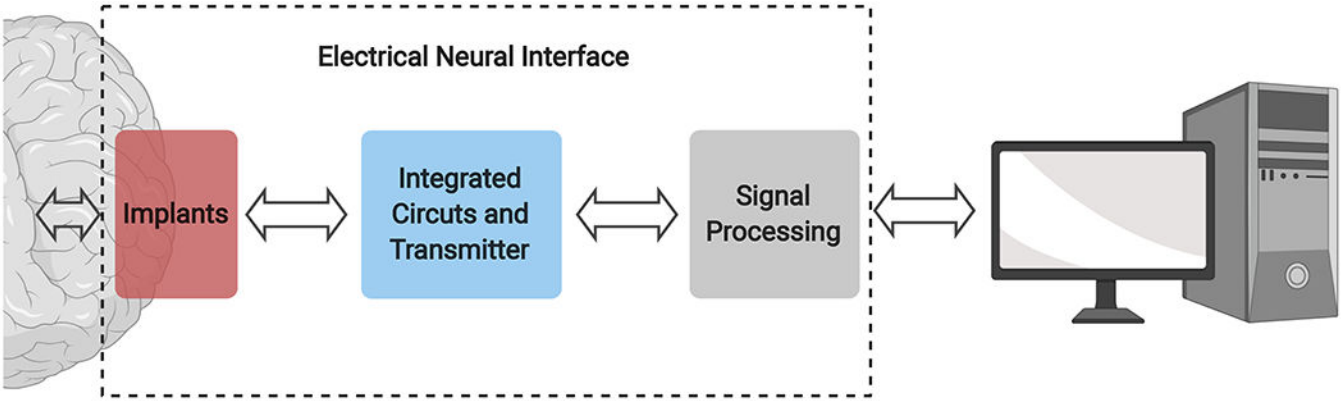

Figure 1.
General construction of an electrical neural interface.

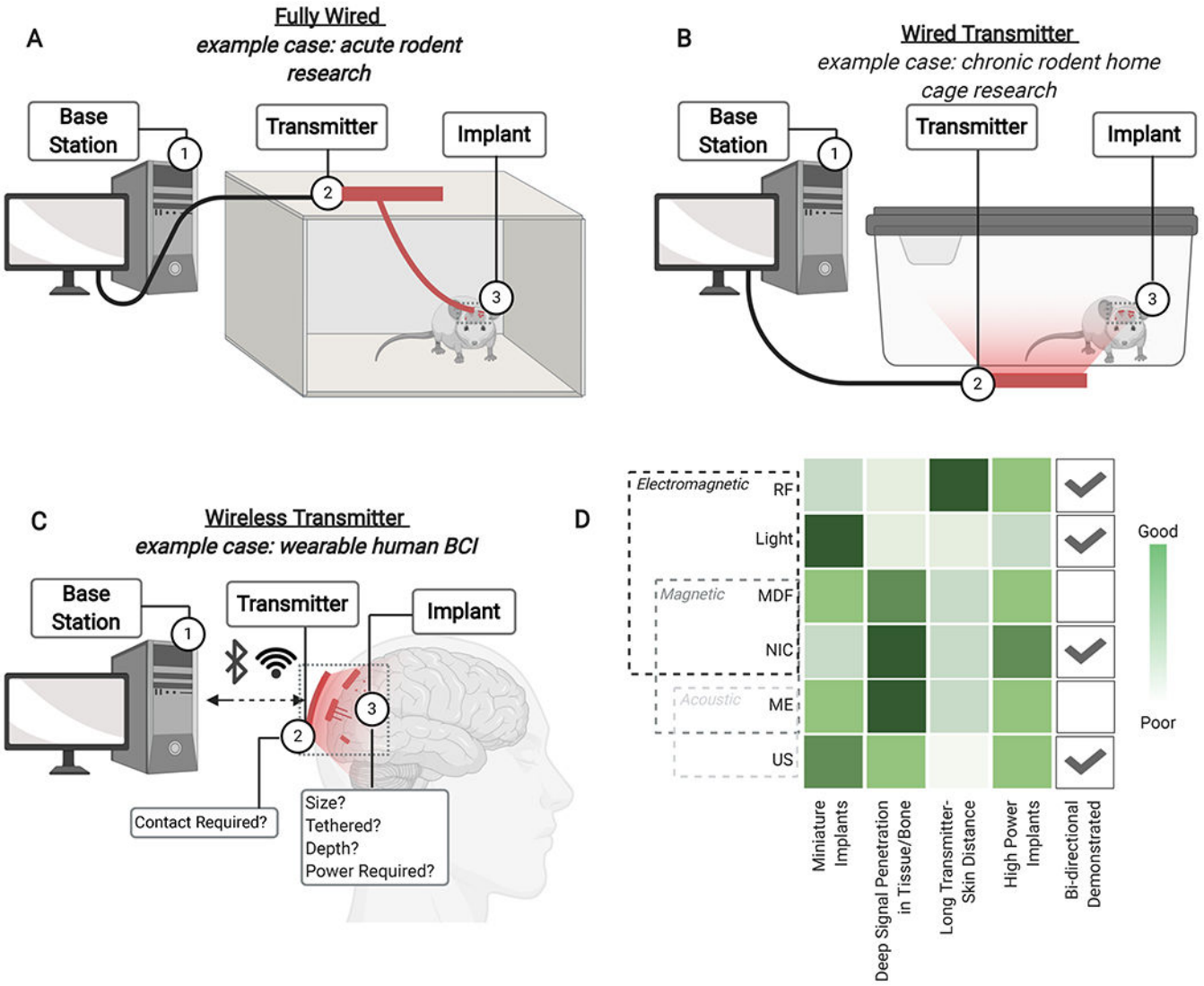

Figure 2. System overview of wireless neural interfaces.

(A) A “fully wired” system, or (B) a “wired transmitter” system generally used with rodent acute or chronic experiments, respectively, or (C) a “wireless transmitter” system, generally used with large animals or humans, which delivers data and power between a base station, transmitter, and implant to specifically control neural stimulation and/or recording. (D) A comparison of the advantages and limitations of different forms of wireless signal between the relay and the implant shows design considerations for next generation wireless systems. Abbreviations: BCI: Brain computer interface, MDF: Mid-field, NIC: Nearfield Inductive Coupling, RF: Radio-frequency electromanetic, US: Ultrasound

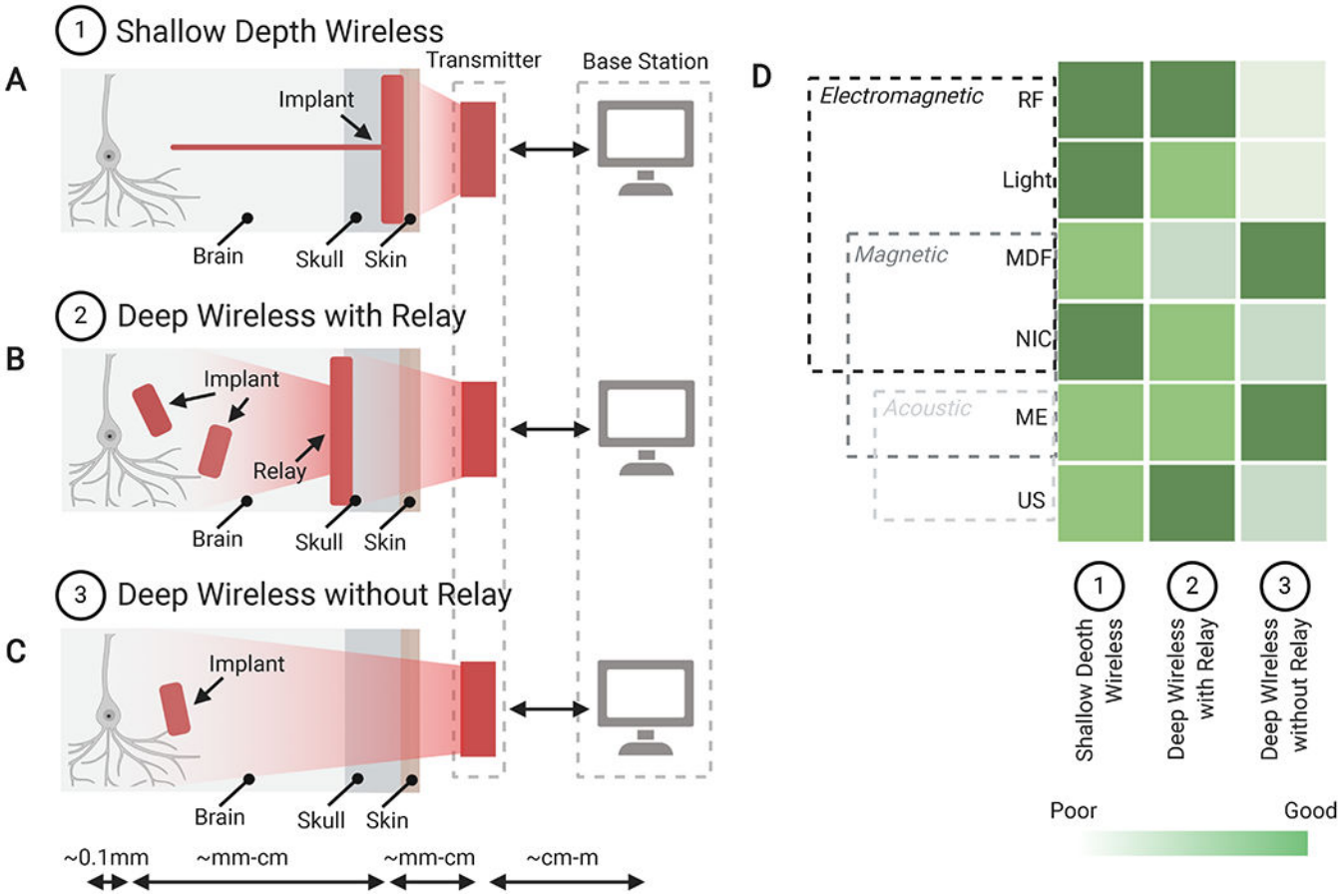

Figure 3. A comparison of Different Wireless Implant Types.

Schematics of experimental configurations that feature a wireless signal sent from a base station and transmitter to: (A) a tethered shallow implant anchored above the skull with an electrode penetrating to deep brain areas; (B) a secondary relay implant projecting wireless signals from the relay to smaller deeply implanted devices; or (C) a deep brain wireless implant. (D) Comparison of the compatibility of different forms of wireless, power-transfer methods for each of the three implant categories, indicating suitable candidates for different implant types. Abbreviations: MDF: Midfield, NIC: Nearfield Inductive Coupling, RF: Radio Frequency, US: Ultrasound.

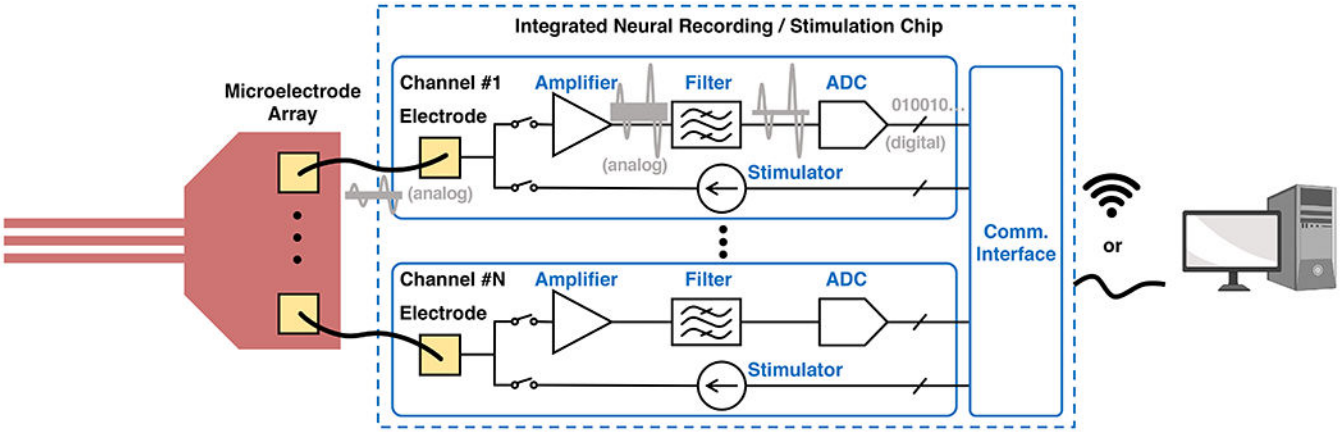

Figure 4. System architecture of the electronics part of a bidirectional neural interface.

In the recording path, the neuronal signals are amplified, filtered, and then converted to binary digital data streams. In the stimulation path, the stimulators generate appropriate stimulation pulses to be delivered by the neural implant. A wireless or wired communication interface sends the recording data to the computer for signal processing and receives the computer commands to program the chip.

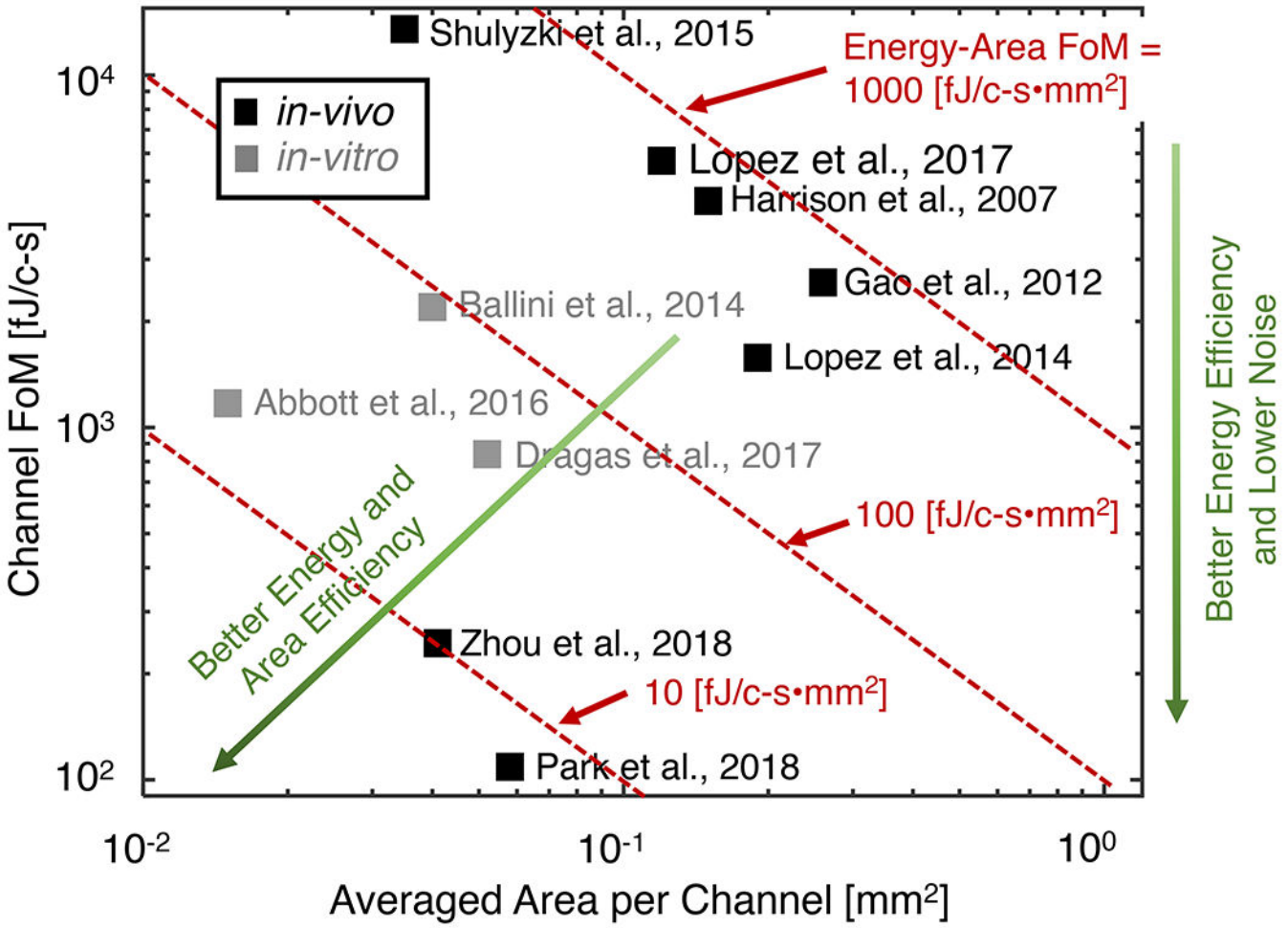

Figure 5. Channel FoM and Energy-Area FoM (proposed in Park et al., 2018) of recently reported neural recording chips.

With a fixed sampling rate, a lower Channel FoM indicates better energy efficiency and lower noise. The second figure of merit, called Energy-Area FoM, evaluates how efficiently both energy and area are used to realize neural recording chips.

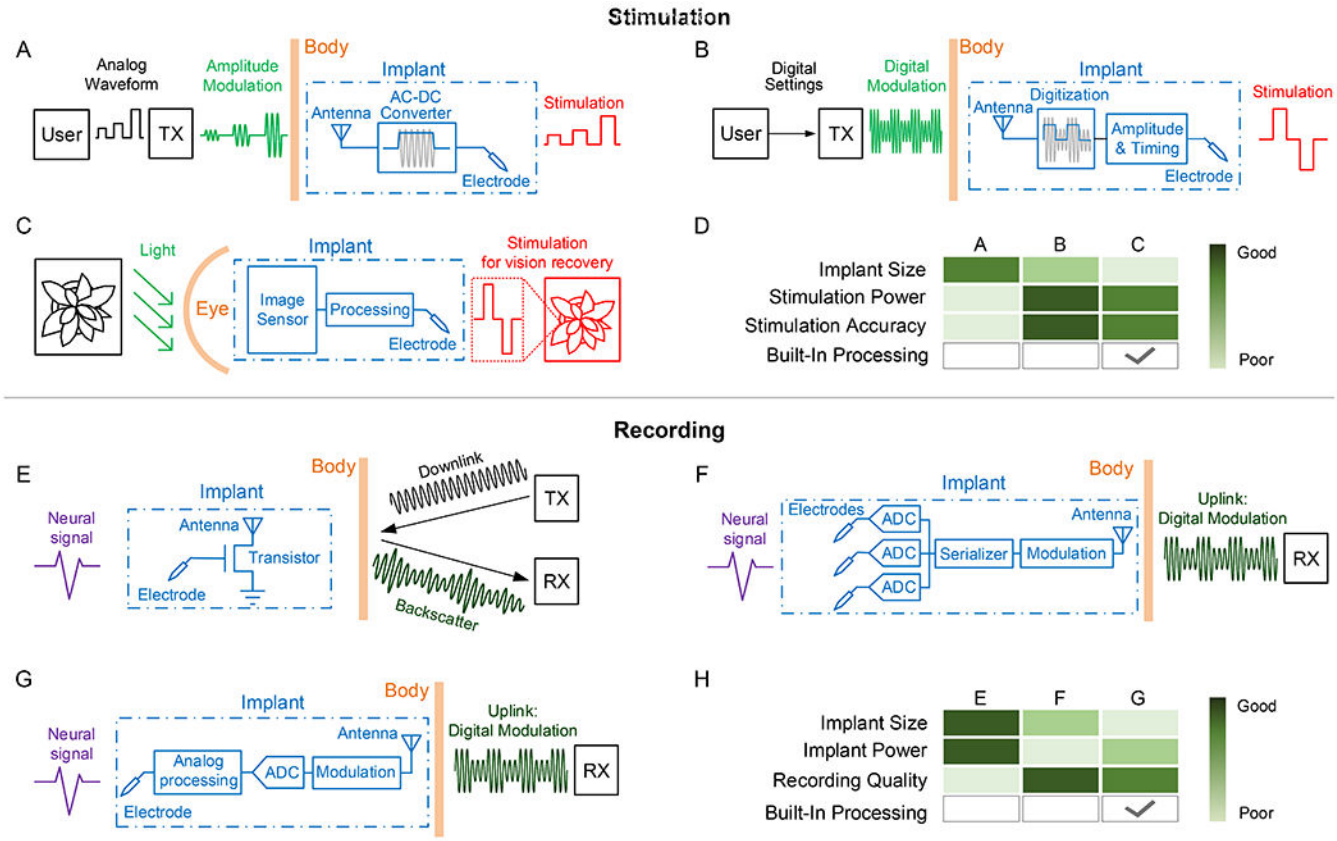

Figure 6. System schemes for neural stimulating and recording implants.

Stimulator schemes with (A) analog programming of stimulation; (B) digital programming of stimulation; (C) sensor-controlled stimulation. (D) A comparison of the above stimulator mechanisms. Recorder schemes with (E) analog backscattering of recorded neural signals; (F) digital communication of locally digitized neural signals, (G) digital communication of locally processed features of neural signals. (H) A comparison of the above recorder design methods.

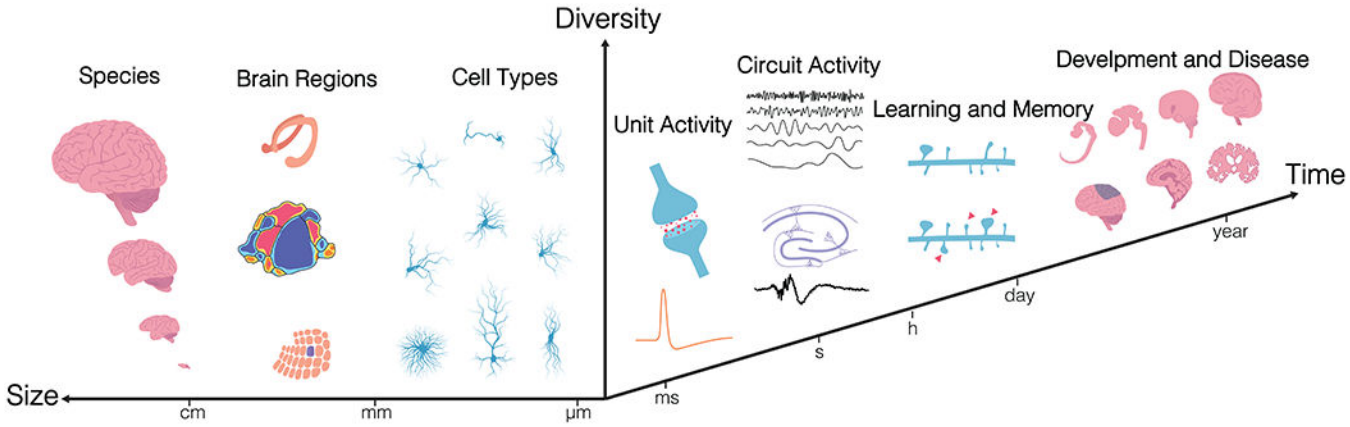

Figure 7. Integration of electrical and optical neural interfaces.

(A) Electrophysiological and optical methods have complementary strengths, in the spatial and temporal resolutions, spatial extent, longevity and number of neurons measured simultaneously. (B) The integration of both methods provides a promising avenue for monitoring large-scale neuronal activity at high spatiotemporal resolutions. Green shading: light. Not drawn to scale. Numbers in (A) derived from (Chung et al., 2017; Jun et al., 2017; Lin and Schnitzer, 2016; Luan et al., 2017)

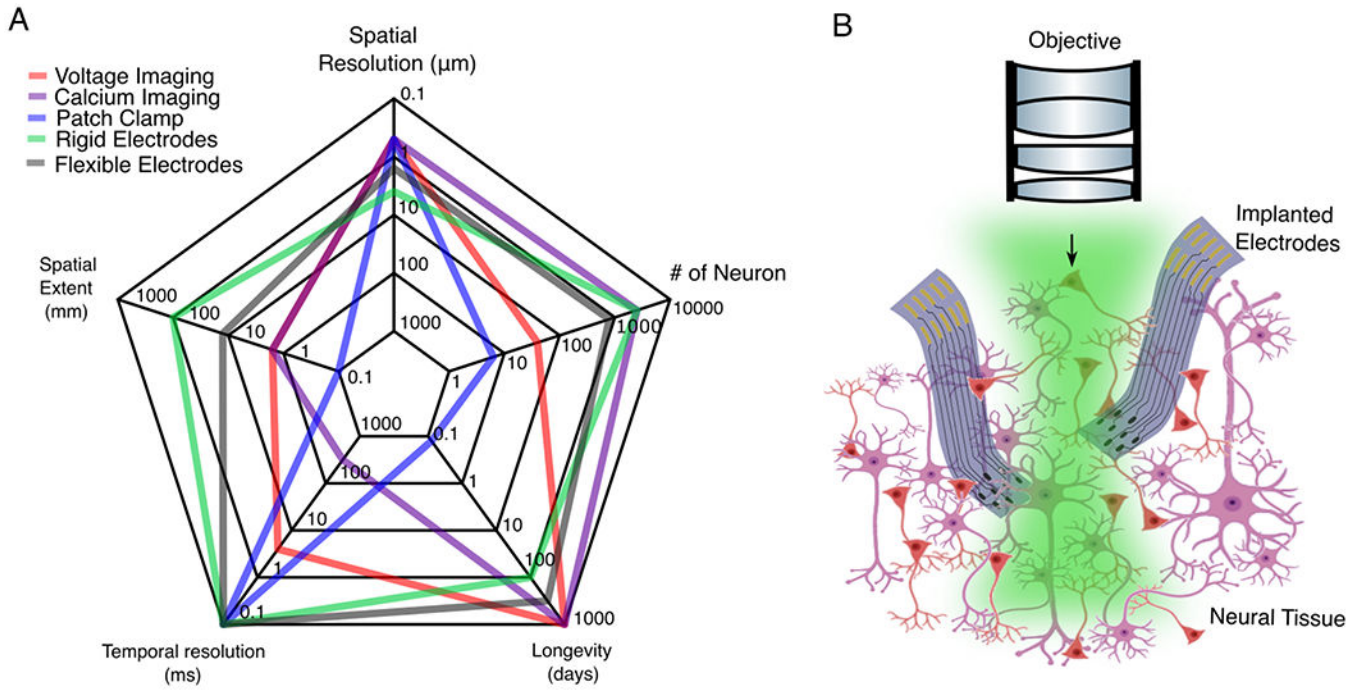

Figure 8: The data-processing pipeline for neural data.

Neural signal is pre-processed for noise removal and filtered into two frequency domains: field potential at lower frequency (<1 Hz to 300 Hz) and spiking activity at higher frequency (300 Hz to 10 kHz). Key techniques are listed in the text.